FRONTIERS OF PHYSICS

TOPICAL REVIEW
Volume 19 / Issue 2 / 23501 / 2024

Recent advances in halide perovskite memristors: From materials to applications

Sixian Liu[1], Jianmin Zeng[1,†], Qilai Chen[2,‡], Gang Liu[1,#]

1 Department of Micro/Nano Electronics, School of Electronic Information and Electrical Engineering, Shanghai Jiao Tong University, Shanghai 200240, China
2 Aerospace Science & Industry Shenzhen (Group) Co. Ltd., Shenzhen 518000, China
Corresponding authors. E-mail: †jamy3531@sjtu.edu.cn, ‡chenqilai8816@126.com, #gang.liu@sjtu.edu.cn
Received May 20, 2023; accepted August 29, 2023

ABSTRACT

With the emergence of the Internet of Things (IoT) and the rapid growth of big data generated by edge devices, there has been a growing need for electronic devices that are capable of processing and transmitting data at low power and high speeds. Traditional Complementary Metal-Oxide-Semiconductor (CMOS) devices are nonvolatile and often limited by their ability for certain IoT applications due to their unnecessary power consumption for data movement in von Neuman architecture-based systems. This has led to a surge in research and development efforts aimed at creating innovative electronic components and systems that can overcome these shortcomings and meet the evolving needs of the information era, which share features such as improved energy efficiency, higher processing speeds, and increased functionality. Memristors are a novel type of electronic device that has the potential to break down the barrier between storage and computing. By storing data and processing information within the same device, memristors can minimize the need for data movement, which allows for faster processing speeds and reduced energy consumption. To further improve the energy efficiency and reliability of memristors, there has been a growing trend toward diversifying the selection of dielectric materials used in memristors. Halide perovskites (HPs) have unique electrical and optical properties, including ion migration, charge trapping effect caused by intrinsic defects, excellent optical absorption efficiency, and high charge mobility, which makes them highly promising in applications of memristors. In this paper, we provide a comprehensive overview of the recent development in resistive switching behaviors of HPs and the underlying mechanisms. Furthermore, we summarize the diverse range of HPs, their respective performance metrics, as well as their applications in various fields. Finally, we critically evaluate the current bottlenecks and possible opportunities in the future research of HP memristors.

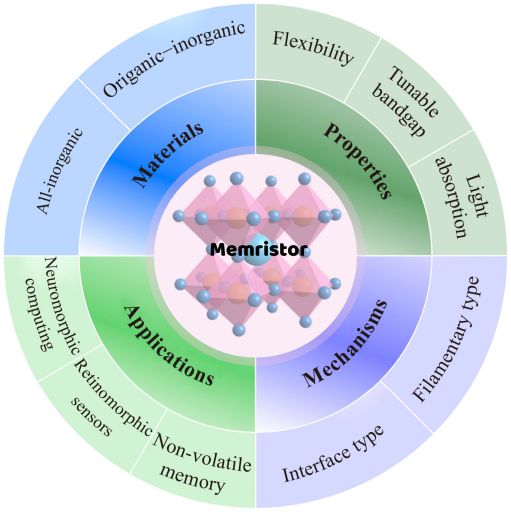

Keywords halide perovskite, memristor, mechanism, neuromorphic computing, non-volatile memory

*Special Topic: Materials, Mechanisms and Applications of Memristors (Eds.: Xiaobing Yan, Bin Gao & Qi Liu).

Higher Education Press

https://doi.org/10.1007/s11467-023-1344-9

Contents

1 Introduction

The advent of the Internet and the Internet of Things (IoT) has transformed people's lifestyles. In the rapidly evolving landscape of computing technology, the traditional von Neumann architecture has long been the predominant paradigm for designing computers, in which storage and computation are separate units [1–3]. However, as technology continues to progress at an unprecedented pace, the limitations of this architecture have become increasingly apparent [4–6]. One of the most significant issues is the memory wall problem, which arises due to the disparity in speed between processing units and memory units. As a result, the performance of a computer is bottlenecked by the transfer of data between the processor and the memory units, leading to slower processing speeds and decreased efficiency, especially in data-intensive applications [7].

Based on different active materials, exploring new integrated systems with higher performance through structural design, preparation optimization, and application expansion is an important research content in the intelligent information world [8–10]. To meet the demands of low power consumption and real-time response, like fire alerts, and unmanned aerial vehicles (UAVs), a delicate balance between computational efficiency and power consumption must be achieved [11, 12]. Unfortunately, this can be a challenging task. Traditional computing units are often restricted by a poor balance of performance, size, and energy consumption, which underscores the need for novel integrated electronic devices to overcome these limitations.

Researchers and engineers have been exploring alternative architectures and memory technologies that can circumvent the memory wall problem to address this challenge. One such technology is memristors, which are nanoscale electronic devices that can store and process data in an identical unit. Memristors, including non-volatile memory devices such as phase change random access memory (PCRAM), ferroelectric random access memory (FeRAM), and conductive bridge random access memory (CBRAM) [13, 14], are considered a potential solution to the memory wall problem due to their unique properties, including high density, low power consumption, long retention time, and high-speed [15–19].

Memristors were first introduced by Leon Ong Chua in the 1970s and are one of the four basic passive electronic components, alongside inductors, resistors, and capacitors. However, they are relatively less known compared to the other three components. Almost 40 years later, experiments finally confirmed the memristor concept in 2008. A team led by S. Williams at HP Research Lab demonstrated that switching resistors between on and off states could show Chua's memristor behaviors in metal oxide thin film devices. They fabricated the first memristor using titanium dioxide thin films and Pt electrodes, which operate based on oxygen vacancy transfer between two layers of TiO_2 in contact with each other [20].

In recent years, to further improve the performance of memristors, the dielectric selection of memristors has become more diverse [1, 21–23]. As early as 2008, Tulina *et al.* [24] prepared devices with resistive switching properties based on perovskite oxides, then many oxides and organic compounds have been successfully used in preparing memristors and showed better performance. Common semiconductor materials have been studied in the construction of memristors, including silicon oxide (mainly SiO_2) [25–28], SiN_x [29–33], metal oxides (such as $LaFeO_3$, $SrCoO_x$, and $SrTiO_3$) [34–40], graphene and related materials (GRMs) [41], metal nitrides (AlN, TiN) [42–44], metal sulfides (Cu_2S, MoS_2) [45–47], MXenes [48–50], and organic electronic materials [51, 52]. Metal oxides also have the advantage of natural stability in the fabrication of memristors, but there are unavoidable inherent oxygen vacancy defects in the oxides, which limit their function as memristors. At the same time, the preparation of these materials often requires the participation of large instruments, or vacuum atmosphere processing such as high-temperature sputtering and annealing, which complicates the manufacturing process of memristors [53]. In addition, although metal sulfides,

MXenes, and organic electronic materials have unique characteristics such as flexibility and large specific surface area, their retention and durability are poor [54, 55], and their preparation processes are often long and complex [56].

In addition to the dielectrics mentioned above, halide perovskites (HPs) are being widely studied because of their rich physical properties. The structure of ABX_3 determines its good composition flexibility, in which any point can be replaced by other substances. Since the emergence of the first study of perovskites in the 1950s [57], the advantages such as adjustable band gap, long carrier diffusion length, strong light absorption, low defect density, and solution method processing have been gradually recognized. The characteristics of simple processing and suitable for large-scale manufacturing provide a solid foundation for its various applications. At present, HPs have become a rising star in the field of electronic devices, and their unique optoelectronic properties have been proven to make revolutionary progress in many fields [58].

In this review, we are committed to introducing the latest development of HP memristors. Although the initial HP materials are considered a leader in the field of solar cells, many experiments have shown that their conductive mechanism will make them one of the most promising materials in the field of memristors [59, 60]. Next, we introduce the conductive mechanism of memristors and pay special attention to the devices based on HP materials. According to the different compositions and grain sizes of HPs, we describe the latest performance advantages and progress of memristors based on many different types of HPs [61]. Since then, the applications of these HP devices have also been considered, including neuromorphic computing, physical unclonable functions (PUF) encryption, intelligent optoelectronic recognition systems, and so on.

Although memristors have the potential to provide the best storage performance (fast and reliable), research into this novel device is still in its infancy. In this context, the discussion will delve into the benefits of using HP memristors as a solution to the memory wall problem, exploring their advantages over traditional memory technologies and how they can be integrated into next-generation computing systems. By providing a comprehensive overview of the state of the art in HP memristors, this review will summarize the future research prospects and possible obstacles based on the current situation of HPs, providing valuable insights into this exciting and rapidly evolving area of research.

2 Properties of halide perovskites (HPs)

Perovskite is a large class of crystals with a three-dimensional structure based on $CaTiO_3$, which mainly includes all-inorganic perovskite materials [62] and

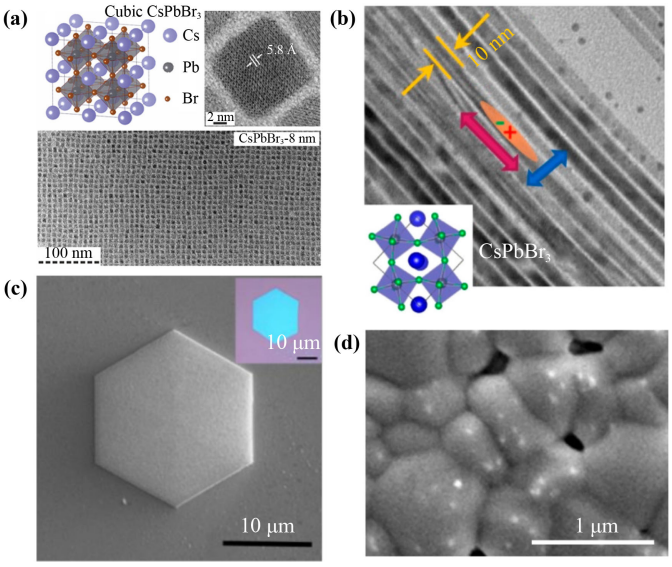

Fig. 1 Classification of perovskite materials according to material dimensions. **(a)** Zero-dimensional QDs. **(b)** One-dimensional nanowires. **(c)** Two-dimensional nanowires. **(d)** Three-dimensional polycrystalline. (a) Reproduced from Ref. [74]. (b) Reproduced from Ref. [75]. (c) Reproduced from Ref. [76]. (d) Reproduced from Ref. [77].

organic–inorganic hybrid perovskite materials. It can exist stably in many forms, such as three-dimensional (3D, crystal), two-dimensional (2D, thin film), one-dimensional (1D, nanowire), and zero-dimensional (0D, quantum dots) [63–66]. As a new type of optoelectronic material, perovskite materials have an appropriate band gap, good charge transfer characteristics, and flexibility. These excellent optoelectronic properties are considered to be necessary conditions for the preparation of excellent optoelectronic devices [66, 67]. Generally speaking, the structure of organometallic trihalide perovskite is ABX_3, where A, B, and X represent an organic cation (MA^+ or $CH_3NH_3^+$), an inorganic cation (Pb^{2+} or Sn^{2+}), and a halide anion (I^-, Br^-, Cl^- or mixed halide), respectively. Organic–inorganic hybrid perovskite has the advantages of the adjustable band gap, high carrier mobility, considerable carrier diffusion length, low-temperature processing technology, low exciton binding energy, optical absorption bandwidth, and so on [64, 68]. Different dopants can be used to adjust the band gap of materials to replace different halide ions.

When the size of the semiconductor grain is reduced to twice or less than its Bohr exciton radius, as shown in Fig. 1, it will show different characteristics from its macroscopic properties in energy level structure, exciton dynamics, and other aspects due to the quantum confinement effect, which is called quantum dots (QDs) or zero-dimensional semiconductor [69]. Compared with bulk perovskite materials, QDs exhibit special optical and electrical phenomena. In addition, the multi-functional surface and relatively free colloid state of perovskite

QDs allow them to be dispersed into various solvents to facilitate the fabrication of optoelectronic devices. At present, perovskite QDs have been commercialized and play an important role in the fields of luminescent devices, fluorescence sensing, and LED display [70]. One-dimensional perovskite nanowires are natural optical cavities and have potential applications in optical waveguides and polarizing devices. In electrical devices, one-dimensional nanowires are conducive to the directional and rapid transport of carriers, which helps to prolong the lifetime of carriers. Two-dimensional perovskite materials have ultra-thin planes and are highly compatible with flexible substrates, making them ideal materials for assembling flexible optoelectronic devices [71, 72]. Compared with perovskite QDs, two-dimensional perovskite nanocrystals have no grain boundaries, which is beneficial to carrier transport in electronic devices and reduces exciton quenching in optical devices. In three-dimensional crystals, compared with single-crystal perovskite materials [73], polycrystalline perovskite films are easy to be prepared on a large scale and have more practical application value.

Based on the above excellent characteristics, HPs have been extensively studied in various optoelectronic devices. In these devices, HPs primarily function as light absorbers and emitters, such as solar cells and photodetector systems. Among the reported photovoltaic materials, perovskite solar cells (PSCs) have become the most promising solar power generation system because of their low cost and high efficiency.

In recent years, it has been reported that the photoelectric conversion efficiency (PCE) of PSCs has made remarkable progress because of its unique and excellent optoelectronic performance, especially since the breakthrough report of solid-state PSCs in 2012 [78, 79]. To be specific, PCE has increased from 3.8% in 2009 [80] to 32.5% in 2023 [81], which has exceeded the high-efficiency thin film solar cells based on CIGS, CdTe, or polysilicon. In addition to photovoltaic applications, HPs have also proven to be effective materials for light-emitting diodes [82–84], X-ray detectors [85], and photodetectors [86, 87]. In 2021, Lee *et al.* [88] reported a world-record-breaking perovskite LED device with an external quantum efficiency of 23.4%, which is comparable to the maximum current efficiency of traditional III–V and II–VI inorganic QDs LED. In 2020, Hu *et al.* [89] reported that the perovskite wafer with the maximum X-ray detection sensitivity has the ability to prepare the largest circular perovskite crystals with a diameter of 8 cm. HPs are showing their amazing adaptability in all directions in the optoelectronic field, and the emergence of these materials will provide more vigorous directions for scientific research.

3 Memristive mechanisms of HP memristors

Due to the rate-dependent hysteresis phenomenon, there have been challenges in accurately measuring the power-conversion efficiency of solar cells, which causes ambiguity in determining the real current–voltage curve with conventional measurement techniques [90]. Taking PSCs as an example, the scanning rate, operational point, and scanning direction all influence the obtained current-voltage curves, resulting in rate-dependent hysteresis [91, 92]. For a long time, researchers in the field of PSCs have made many attempts to eliminate the hysteresis effect of photocurrent, including stabilizing the material structure by component engineering [93], reducing traps and selecting a suitable electron transport layer [94]to optimize the charge transport process. To explain this phenomenon, mechanisms such as ferroelectricity [95], charge trapping [96, 97], and ion migration [98, 99] have been proposed. The interface between active metal and perovskite materials is not desirable in typical PSCs, as it causes current hysteresis which leads to inaccurate cell efficiency and reduces the overall photovoltaic performance [100]. However, current hysteresis is a fundamental requirement for memristor resistive switching behaviors [101], and the above conductive mechanism and chemical activity can be applied in memristors. Memristors, short for memory resistors, are a type of non-volatile memory device that can change their resistance in response to applied electrical stimuli. They have shown great potential in a wide range of applications, such as neuromorphic computing, logic circuits, and energy-efficient data storage. Memristors are still a rapidly developing field of research, with ongoing efforts to improve their performance, reliability, and scalability for practical applications. According to the mechanism of HP memristors, resistive switching can be roughly divided into filamentary and interface-type switching.

3.1 Filamentary resistive switching (FRS)

The resistive switching behavior of filament memristors comes from the formation and fracture of conductive filaments, which can be divided into three types according to their formation rules, including electrochemical metallization (ECM), valence change mechanism (VCM), and thermochemical memory effect (TCM) [102, 103]. Among them, TCM is a common resistive switching mechanism related to unipolar memristors with active electrodes. Under the current flow, the generation of Joule heat will lead to the accumulation of local heat, which alters the stoichiometric ratio of HPs and causes a change in conductance. Because the generation of Joule heat is independent of the direction of the applied voltage, it is mainly suitable for unipolar devices. A higher reset current is often required to increase the temperature of the conductive filament, resulting in its fusion by Joule heat and transfer back to a high resistance state (HRS) [104, 105].

For most bipolar devices, the conductive filaments

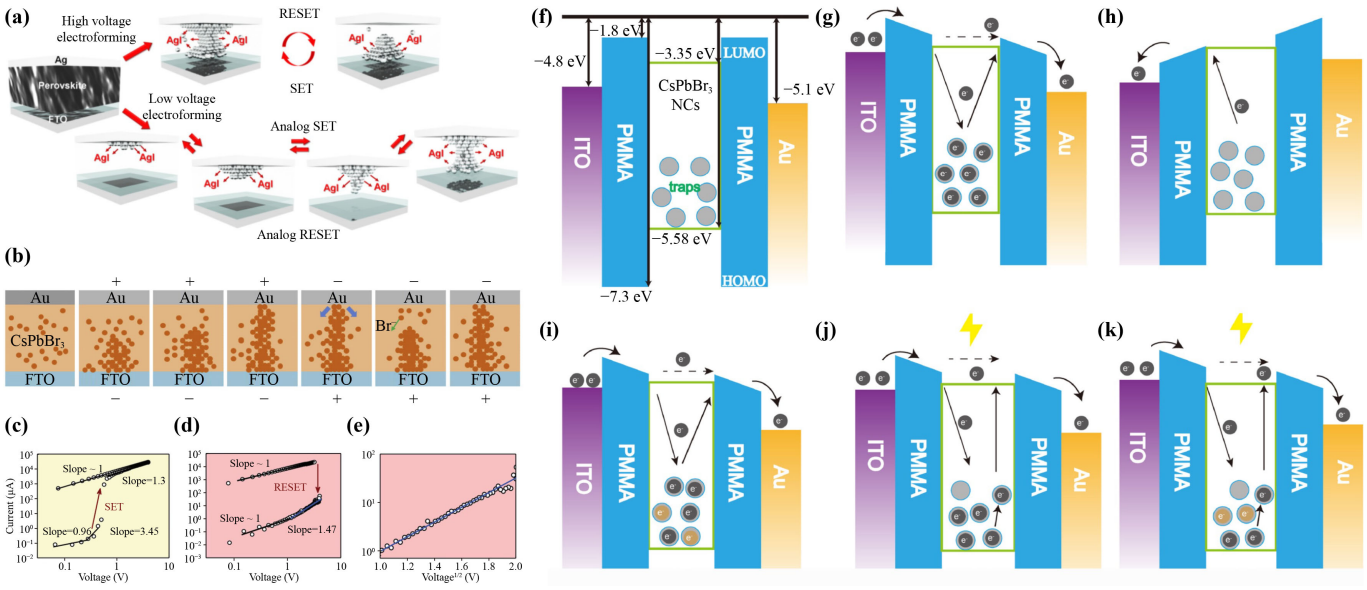

Fig. 2 **(a)** The resistive mechanism of the Ag/$CH_3NH_3PbI_3$/FTO memristor, in which the upper part of the process involves the electroforming process. **(b)** Schematic diagram of the filamentary memristors. **(c)** Current–voltage characteristics of the "set" process in double-logarithmic scale. **(d)** Current–voltage characteristics of the "reset" process in double-logarithmic scale. **(e)** The relationship of I and $V^{1/2}$ in the LRS semi-logarithmic scale in the high voltage region. A schematic diagram of the band evolution corresponding to various states of the device. **(f)** Initial state and HRS-1 state. The device change **(g)** from HRS-1 to LRS, **(h)** from LRS to HRS-1, and **(i)** Transition from HRS-2 to LRS. **(j)** Optical response of devices in HRS-1 and **(k)** HRS-2. (a) Reproduced from Ref. [112]. (b) Reproduced from Ref. [115]. (c) Reproduced from Ref. [76]. (c–e) Reproduced from Ref. [117]. (f–k) Reproduced from Ref. [123].

mostly follow the mechanism of ECM and VCM [106]. The ECM mechanism usually occurs in the memristors with the structure of active electrodes/HPs/inert electrodes, where the conduction pathway at the interface is caused by the use of active metal electrodes. Active electrodes such as Ag and Cu are often used as top electrodes. Under the action of an external electric field, active metals will be oxidized and dissolved into cations [107, 108]. Subsequently, these ions continue to migrate to the HPs layer under the action of an external electric field until they come into contact with the bottom electrodes, and the solid metal atoms are reduced by an electron collision reaction. The gradual accumulation of metal atoms from the top electrode to the bottom will form a path between the electrodes, which promotes communication between them, resulting in a sudden decrease in the resistance of the device, which is the "SET" state or low resistance state (LRS) in the memristors. Under the applied reverse voltage, on the one hand, the metal cations will migrate in the opposite direction; on the other hand, Joule heat will also promote the fracture of conductive filaments, and the device will be returned to the HRS by "RESET".

Conductive filament distribution and variability are the main factors that limit the multi-stage storage function in FRS behavior. Memristors with only two stable states (HRS and LRS) are commonly used for on/off control or binary storage, such as those studied by Yoo *et al.* on $CH_3NH_3PbI_{3-x}Cl_x$ [109], Choi *et al.* on $CH_3NH_3PbI_3$ [110], and Lee *et al.* [111]. However, the formation of a special crystal phase will also enable some devices to acquire the ability of multi-stage storage. In 2018, Ku *et al.* [112] explored the potential of (CH_3NH_3) PbI_3 as the active layer of synaptic devices, where the generation/fracture of conductive filaments caused by Ag as the top electrode is the main reason for the resistance behavior. After seven consecutive 0.2 V DC voltage scans on the Ag top electrode, the current level increases gradually. The resistive switching behavior is classified as an analog memristor, as it slowly varies over time, unlike the digital memristor from HRS to LRS. The AgI layer acts as the warehouse of Ag atoms, which are released gradually with the increase of external stimulation [Fig. 2(a)], and the simulation of multi-stage resistance is realized [112].

Due to the inherent defects in HPs, the redistribution of these defects under the applied electric field will also lead to changes in electrical conductivity, which is called VCM and a common mechanism of most metal HP memristors. Electrochemical redox and anion vacancy migration play an important role in the formation and fracture of conductive filaments [113, 114]. The electrodes mainly serve as electrical conductors and do not participate in the reaction. The migration and diffusion of the defects formed by the HP film play a leading role in the formation of conductive filaments. The composition of perovskite is often limited to stoichiometry, in which

many inherent defects will be formed, and their formation energy is the smallest and is most easily affected by an external electric field. The migration will be accelerated by the diffusion and drift component field. The all-inorganic polycrystalline $CsPbBr_3$ thin film memristor developed in 2019 is an example of VCM [Fig. 2(b)]. The migration of inherent Br defects in polycrystalline perovskite contributes to the formation of conductive filaments, and the bromine vacancy will move along the edge of the shared octahedral structure, which leads to the formation and decomposition of conductive filaments [115]. In 2020, Ge *et al.* [116] used lead-free low-dimensional perovskites $Cs_3Bi_2I_9$ and $CsBi_3I_{10}$ to create resistive memory with an ultra-low operating voltage of 0.1 V. Paramanik also achieved high-performance memristors using $Cs_3Sb_2I_9$ with a switching ratio of 10^4 and VCM as the conductive mechanism. The device switches from HRS to LRS by forming conductive filaments through iodine vacancy defects under positive pressure, as shown in Figs. 2(c–e), and remains in LRS until the filament breaks upon reversal of the voltage [117].

In conclusion, FRS mechanisms in HP memristors have shown great potential for next-generation memory devices [118]. TCM is a relatively new FRS mechanism with superior performance, but its scalability may be limited by the requirement for a high-temperature pulse. ECM has been extensively studied and demonstrated excellent performance, but its reliability is a concern. VCM has shown promise in achieving uniform filament formation, but its low on/off ratio and slow switching speed limit its practical applications. Further research is needed to address these limitations and to optimize the performance of HP memristors for practical applications.

3.2 Interface-type resistive switching (ITRS)

In the interface-type memristor, HPs are usually used as the functional layer to establish the Schottky contact between the electrodes. The process of interface charge movements such as charge trapping and de-trapping, accumulation, and anion migration of the insulating layer near the electrode is the root cause of the change in Schottky barrier height [119, 120]. Finally, the resistance can change with the adjustment of the Schottky barrier height at the interface and is strongly related to the area. This device structure will also form a p–i–n junction, which may lead to a change of capacitance [59].

This mechanism has been demonstrated in various perovskite materials, such as $CsSnI_3$ [121] and $CsPbI_3$ [122]. For instance, in 2019, Zhang *et al.* [123] made an ITRS memristor based on $CsPbBr_3$ nanocrystals (NCs), which achieved two HRS states and one LRS state. Under forward voltage, charge carriers injected through the positive electrode (Au) are continuously captured until the maximum capacity is reached. The potential barrier between the gold electrode and PMMA is weakened, allowing electrons to pass through and be trapped by the NCs [Figs. 2(f, g)]. Conversely, applying negative voltage transfers the trapped electrons back to the ITO, transitioning the device back to HRS, as shown in Figs. 2(h, i) [123]. Also, light-induced carriers can help the transition process shown in Figs. 2(j, k). In terms of the mechanism model, the conduction mechanism of ITRS memristors usually uses some models to fit the I–V curve, such as space charge limited current (SCLC, $\ln(1/E) \propto E$) [124, 125], Schottky emission (SE, $\ln(J/T^2) \propto T^{1/2}$) [126, 127], Poole–Frenkel emission (PF, $\ln J \propto E^{1/2}$) [127], trap assisted tunnelling (TAT, $\ln J \propto 1/E$) [128], thermionic emission (TE, $\ln(J/T) \propto 1/T$) [129, 130], and Fowler–Nordheim tunnel (FNT, $\ln(J/E^2) \propto 1/E$) [128], where J represents for current density, E represents for the electric field, and T represents for temperature.

ITRS perovskite memristors typically require lower switching voltages, leading to lower power consumption and longer device lifetime [131]. Also, without the restrictions of filament distribution, ITRS perovskite memristors can be fabricated in a smaller size, enabling a higher density of memristor arrays. Additionally, ITRS perovskite memristors exhibit good uniformity in terms of switching voltages and resistive states, making them suitable for large-scale integration. However, one major limitation of ITRS perovskite memristors is their lower on/off ratio compared to FRS perovskite memristors. This can lead to lower memory reliability and limit their use in some high-performance demanding applications. Another limitation is their limited endurance due to the accumulation of ion vacancies and other defects that can degrade the switching performance over time. Overall, ITRS perovskite memristors show promise for high-density memory applications, particularly in low-power and large-scale integration applications [132]. However, at present, the research on memristors is still based on FRS memristors because of their advantages in endurance. In the future, the potential application of ITRS memristors in the construction of hardware-based artificial neural networks (ANNs) and further research should also be considered.

4 HP memristors

Understanding the memristive mechanisms is not only crucial for exploring the vast potential of memristor devices but also serves as the cornerstone for effectively classifying HP memristors based on their dimensions and components. By gaining insights into the underlying principles that govern resistive switching, we can establish a strong and coherent link between the theoretical foundations and the practical categorization of HP memristors. With this solid understanding of the memristive mechanisms in place, we now direct our attention to the classification of HP memristors based on their components and dimensions. We divide the discussion into three main categories: three-dimensional HP memristors, low-

dimensional HP memristors, and multi-dimensional HP memristors. Within each category, we further examine the distinct subtypes. We present a systematic account of the recent advances and emerging applications of HP memristors across various dimensions, which enables us to explore the diverse landscape of HP memristors, elucidating their unique characteristics and applications.

4.1 Three-dimensional HP memristors

Most HPs have a 3D structure, the general formula is ABX_3, and its structure consists of an octahedral anion network with a shared angle. The octahedron is generated by a simple cubic arrangement of bivalent B-site cations and bridged by halide anions. Univalent A-site cations occupy the cubic octahedral cavity in the B-X sublattice, providing charge balance [133, 134]. The direct band gap semiconductor properties of typical 3D lead HPs are due to the valence band maximum (VBM) being mainly composed of halide p orbitals and Pb s orbitals, while the conduction band maximum (CBM) mainly has the characteristics of Pb p orbitals [135, 136]. A-site anions usually do not participate in the band extrema but still contribute to the electrical properties through the interaction between the organic and inorganic components.

Defect participation is usually required for the formation of conductive filaments or charge transfer in resistive switching behaviors. The defect tolerance of 3D HPs reduces the influence of lattice defects on their electrical properties, enhancing their efficiency and stability in devices. This enables the preparation of large areas of polycrystalline thin films through a simple spin coating method at low temperatures [137]. By precisely controlling the crystallization and morphology of 3D HPs, researchers can optimize their electronic properties and tailor them for specific applications. For instance, recent research has demonstrated that the crystallization of HPs or highly ordered thin films can lead to enhanced charge transport, reduced trap states, and improved stability. These properties are crucial for the development of high-performance electronic and optoelectronic devices such as memristors, logic, sensors, and photovoltaics [138, 139]. The fine control of the crystallization and morphology of 3D HPs has shown it to be a strong candidate for intelligent information devices in the future.

4.1.1 Organic–inorganic HP (OIHP) memristors

In the structure of ABX_3 in OIHP, the A site is generally organic cations such as methylamine (MA), formamidine (FA), and guanidium (GA). In the past few years, OIHPs have made remarkable achievements in the photovoltaic field because of their high carrier mobility, tunable bandgap, and strong light–matter interaction [140, 141]. An in-depth understanding of the physical and chemical properties of OIHPs has promoted the rapid improvement of its application in memristors. 3D OIHPs are the first perovskite material used in memristors. The strategy of mixing various A-site cations to synthesize OIHPs based on double, ternary, and quaternary cations has also been applied to develop efficient resistive switches in these memristors [142].

Memristors based on OIHP materials have been the subject of increasing research in recent years. In 2015, Yoo *et al.* [109] first confirmed the potential of perovskite materials to achieve resistive switching behaviors based on $MAPbCl_3$. Since then, various OIHP materials have been investigated in the field of memristor research. In 2018, Liu *et al.* [143] demonstrated memory write, read, and erase functions in $MAPbI_3$ perovskite devices. This resulted in a simple 0–1 storage example using ion adsorption/desorption generated by interface chemical functional groups for the first time and opened new avenues for nonvolatile memory devices. More recently, Gupta *et al.* [144] proposed a memristor structure without the hole transport layer (HTL) based on the same material. Their device, which used meso-TiO_2 and SnO_2 layers as electron transport layer (ETL) layers in a Glass/ITO/SnO_2/m-TiO_2/$CH_3NH_3PbI_3$/Au device structure, showed good biological function. The proposed structure also improved the tolerance, stability, and uniformity of the device. The production process opened the way for power-on-chip memristors. In addition, Haque *et al.* [145] studied the ion migration characteristics of $MAPbI_3$ in three-terminal devices, which could help researchers further optimize the performance of perovskite-based memristors. In 2023, Kim's group [146] simulated artificial nociceptors using the intrinsic ion mobility properties of OIHPs, demonstrating four important characteristics of artificial nociceptors, such as threshold, nonadaptation, relaxation, and sensitization. This research highlighted the potential of OIHP-based memristors emulating the functionality of biological nociceptors, providing valuable insights for the development of novel sensing and neuromorphic systems.

In 2020, the memristor made by Yang *et al.* [147] based on $MAPbI_3$ can complete more than 1000 continuous modulation states, enabling the construction of a leakage integral and flame (LIF) biologically inspired neuron for the first time. The designed LIF model successfully simulates the functions of biological neurons, and the third-generation ANN is realized at the hardware level. The author demonstrates a simple LIF model by combining the OIHP-based memristor with some peripheral circuits. Figure 3(a) schematically shows the biological neuron of the LIF model and its corresponding experimental circuit implementation [148, 149]. This represents a milestone in the field of ANNs and opens up new possibilities for the development of intelligent information devices in the future. The author has made progress in developing HP memristors that can achieve various modulation states and hardware implementation of the

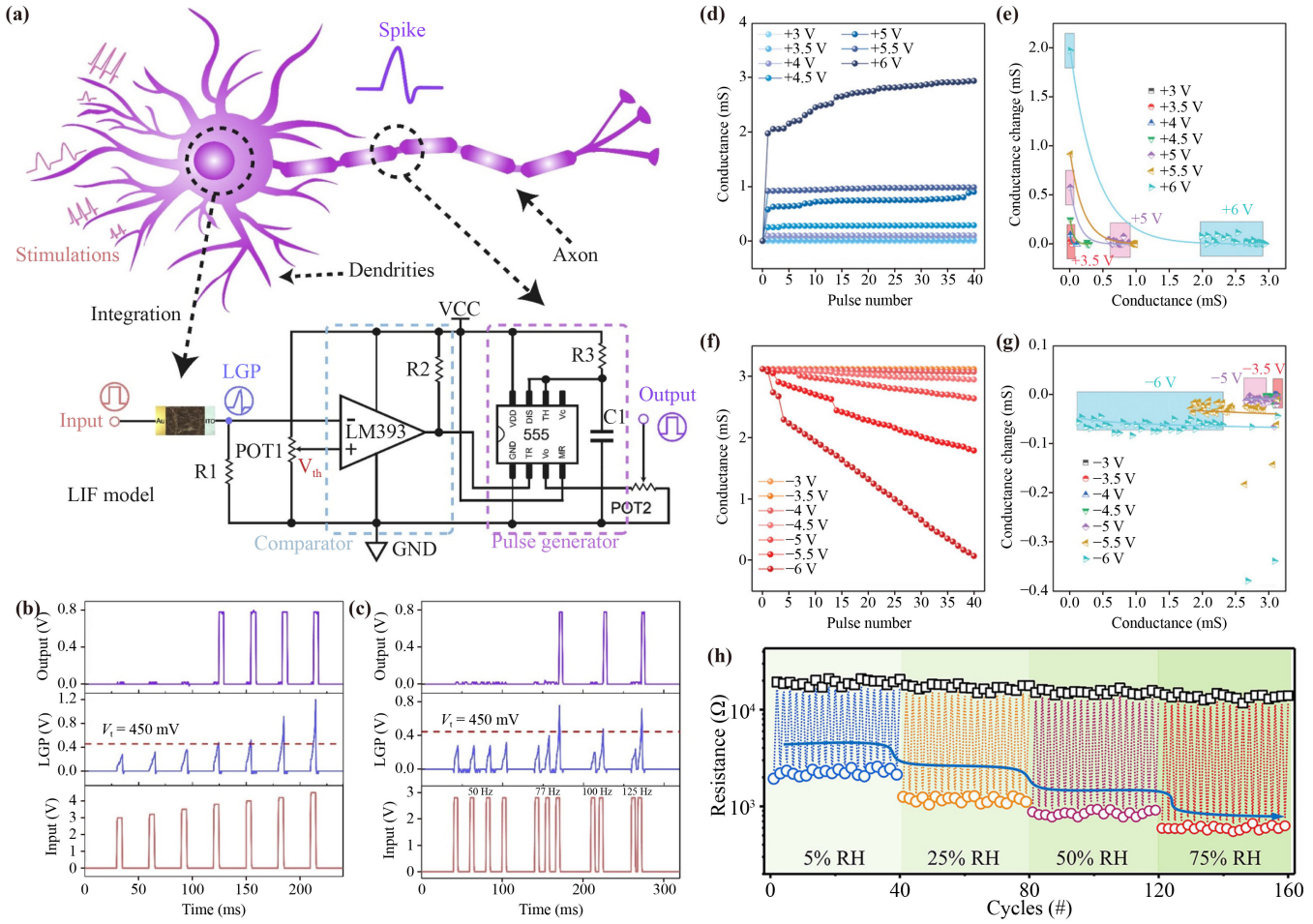

Fig. 3 **(a)** Schematic diagram of biological neurons and their experimental circuits. Using the above neuron model to demonstrate biologically inspired **(b)** Spatial integration and fire. **(c)** Time integration and fire. **(d)** Conductance changes under the same set of pulses stimulation. **(e)** The function of the increment of conductance and the value of absolute conductance (under the condition that the conductance is enhanced). The functional relationship between the change of conductance and **(f)** the number of reset pulses. **(g)** The level of absolute conductance (under the condition of suppression). **(h)** The HRS/LRS distribution of the memristor in pulse programming mode under different humidity. (a–c) Reproduced from Ref. [147]. (d–g) Reproduced from Ref. [151]. (h) Reproduced from Ref. [157].

spiking neural network (SNN) [147]. The improvement of the adaptability, scalability, and fault tolerance of LIF neurons, as shown in Figs. 3(b, c), shows the potential of OIHP materials for mimicking the functionality inspired by human brains. The use of OIHP materials for memristor-based ANNs holds great promise for a new frontier in the field of artificial intelligence and the development of more advanced and intelligent information devices.

In recent research, Sensory synapses based on OIHP memristors have been developed to recognize various external stimuli and transmit nerve signals similar to biological sensory nerves [150]. Sensorimotor neuroelectronics based on OIHP memristor have been used to trigger motor responses in muscles like biological sensory and motor nervous system responses. In 2021, researchers at Nanyang University of Technology [151] fabricated artificial synapses and nociceptors using different HTLs on $MAPbBr_3$ with ion-electronic properties. This is the first report of diffused HP memristors and artificial nociceptors, as shown in Figs. 3(d–g). The authors integrated HP nociceptors and synapses with CMOS neurons for the first time, and demonstrate a typical sensory signal computing platform, which can detect harmful pressure stimuli, representing significant advances in HPs and ionized electronic memristor materials [151].

In the same year, Das synthesized $FAPbBr_3$ and successfully mimicked a series of synaptic behaviors in the $Al/FAPbBr_3/ITO$ structure. These synaptic characteristics are attributed to the electric field-driven migration of halide ions and vacancies in OIHP films [152]. Wang *et al.* [153] have fabricated devices with $FTO/TiO_2/Cs_{0.05}(FA_xMA_{1-x})_{0.95}PbBr_yI_{3-y}/Al$ structure, which have made progress in HP memristors with hybrid A-site and B-site ions, showing optoelectronic properties at a low

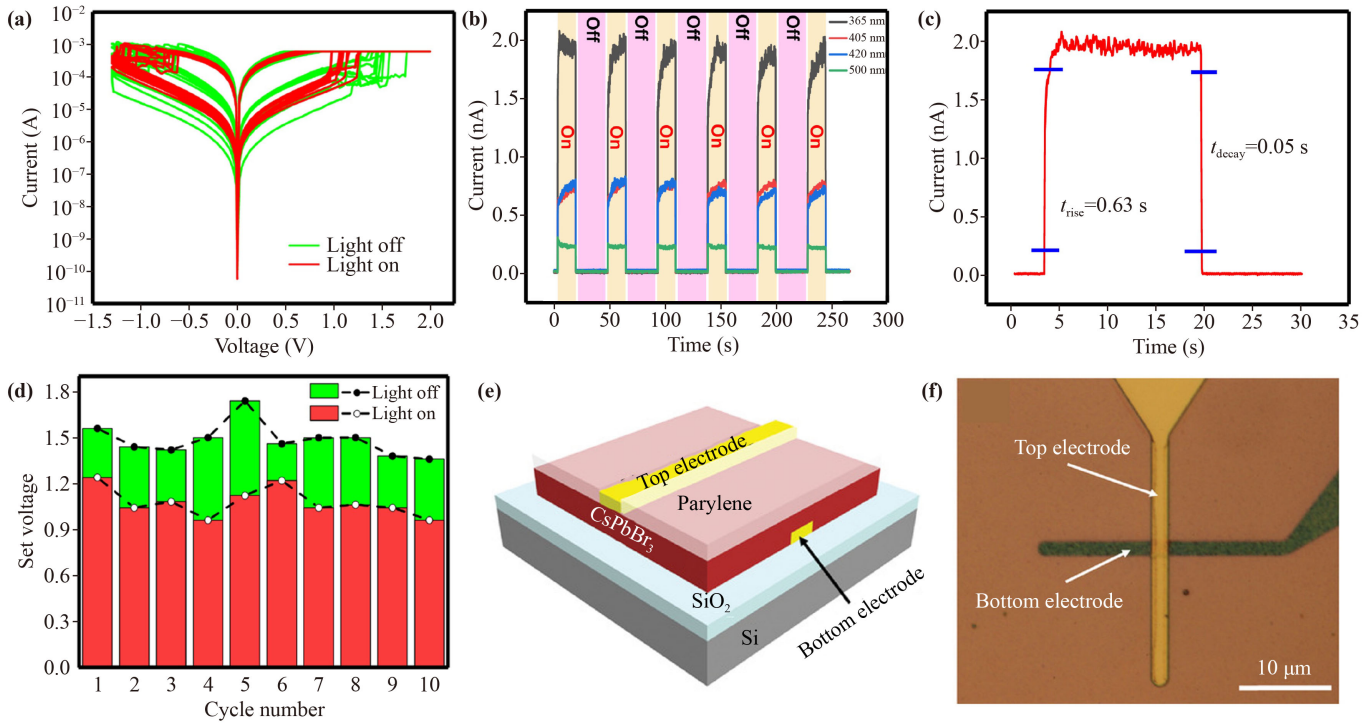

Fig. 4 **(a)** *I–V* curve in light (365 nm) and dark conditions. **(b)** Light response with and without laser diodes at 365 nm, 405 nm, 420 nm, and 500 nm. **(c)** Rise and decay time of light response under 365 nm. **(d)** Set voltage statistics in light (365 nm) and dark conditions. **(e)** Schematic diagram structure and **(f)** optical image of $CsPbBr_3$-based memristor. (a–d) Reproduced from Ref. [123]. (e, f) Reproduced from Ref. [162].

power consumption of ~10^{-9} W.

Additionally, the environmental and thermodynamic stability of OIHP-based memristors is two major challenges that need to be addressed. While water, oxygen, and heat can contribute to its decomposition, appropriate humidity has a positive effect on the OIHP memristors. Water molecules on the HPs surface can fill carrier surface trap mechanisms and improve the conductivity of thin films [154]. Appropriate humidity will improve the performance of the device [155, 156]. In 2021, Zhang *et al.* [157] studied the effect of humidity on Au/$CH_3NH_3PbI_3$/FTO memristor and found that increasing humidity from 5% to 75% decreased the LRS of the device continuously while keeping the HRS unchanged [Fig. 3(h)], leading to an increase in the switching ratio. However, after the humidity increases to 90%, the resistive state retention of the device collapses rapidly and completely dissolves in 3 minutes. This humidity-sensitive resistive switching behavior has potential applications in sensing and safety inspection.

In conclusion, OIHP memristors have shown great potential as a novel type of memristive device due to their unique electronic and ionic properties, low cost, and simple fabrication process. The development of OIHP memristors has led to significant advances in various fields such as neuromorphic computing, in-memory sensing, and energy storage. However, there are still many challenges that need to be addressed, such as environmental and thermodynamic stability, scalability, and integration with existing electronic systems. Further research and development are needed to overcome these challenges and fully unlock the potential of OIHP memristors. With continued efforts, OIHP memristors are poised to become key players in the next generation of advanced electronic devices.

4.1.2 All-inorganic HP memristors

The stability of OIHP memristors is inferior under humid conditions and ambient atmosphere, which can be improved by using all-inorganic HPs material [158, 159]. All-inorganic HPs are currently recognized as the most stable type of perovskites [74, 160, 161]. In 2019, Zhang *et al.* [123] made a nonvolatile memristor with a structure of Au/PMMA/PMMA: $CsPbBr_3$ NCs/PMMA /ITO, which demonstrated the behavior of resistive switching with a ratio up to 10^5 shown in Fig. 4(a). The resistive behavior was attributed to the jump of electrons between capture centers and the ionization of the trapped charges. Under illumination, the photoresponsive currents are high, and the response speed is fast, as shown in Figs. 4(b, c). The photosensitive behaviors of $CsPbBr_3$ NCs help to reduce the operating voltage and power consumption of the device, as shown in Fig. 4(d) [123]. The researchers also fabricated a memristor with a line width of 2 μm by CMOS process, demonstrating the

integration capability of HPs. As illustrated in Figs. 4(e, f), the innovation of the process lies in the use of parylene as a protective layer, which enables HPs to adapt to the harsh environment of lithography and development. This soft packaging process is compatible with CMOS, improving the stability of the HPs layer in the air and establishing a broad prospect in the application field of HPs-based electronic information devices [162].

In 2021, Liu *et al.* [163] developed a $CsPbBr_xI_{3-x}$-based memristor with a retention time of 10^4 s in an ambient atmosphere at 510 K. They improved the thermal stability of HPs by adjusting the stoichiometric ratio of bromide ions. The $CsPbBr_2I$ memristors demonstrated tolerance to temperatures of up to 540 K and could perform electronic read, write, and erase functions at 370 K, thereby expanding the range of applications for HP devices and enabling them to operate in extreme environments to handle more complex tasks [163]. In 2023, the $Cs_2AgBiBr_6$-based memristors with a three-level memory state were prepared and able to maintain stable performance for a period of one-year [164].

Despite having lower photoluminescence quantum efficiencies and shorter photoluminescence lifetime than the best OIHPs, all-inorganic HPs have demonstrated satisfactory stability, particularly thermal stability. Unlike OIHPs, all-inorganic HPs are capable of withstanding high-temperature treatment due to the absence of MA^+ and FA^+ organic cations. This characteristic of all-inorganic HPs makes them an attractive candidate for electronic devices applied in harsh environmental conditions such as extreme temperatures, humidity, and light exposure.

4.1.3 Lead-free HP memristors

Lead is an essential element in the preparation of HPs, but toxicity concerns have driven research into alternative elements for preparing HPs [165, 166]. Bi ion is a popular substitute element for Pb since its radius is similar to that of Pb ion and does not disrupt the crystal phase of HPs [167, 168]. Additionally, other elements such as Ge [169], Cu [170], Sb [171], and Sn [172] have also been extensively studied.

Doping lead-based perovskite materials with alternative elements can also reduce the content of Pb^{2+}. For instance, Ge *et al.* [173] achieved long-term stable and uniform resistive switching behaviors by doping Bi^{3+} into the $CsPbI_3$, which stabilized the cubic lattice and enabled multi-stage HRS for the first time. Similarly, Ruan *et al.* [174] also greatly improved the stability of HPs by doping Bi, which increased the switching ratio of LRS to HRS by 4 orders of magnitude.

Lead-free HP memristors have also been explored, such as iron-based materials with perovskite-like structures. In 2016, Lv *et al.* [175] investigated their resistive switching behaviors and observed a hysteresis window in the voltage scan, with a resistive state maintained at a small read voltage even after 100 V voltage is removed. The interface effect is attributed as the main contributor to the conductance state change behavior of the Ag/$(CH_3NH_3)_2FeCl_4$/Cu memristor. To study the reliability of the device, the effects of temperature changes between 290 K and 340 K on HRS and LRS are tested and shown in Figs. 5(a, b). As the sampling temperature increases, the HRS and LRS may exhibit some fluctuations but remain distinguishable from each other [175].

Besides, there have been several studies showing potential for practical applications in neuromorphic computing and flash memory based on lead-free HP memristors. Yang *et al.* [176] demonstrated the synaptic characteristics of $MA_3Sb_2Br_9$ memristors for the first time [Fig. 5(c)] and paved the way for lead-free HPs in neuromorphic computing. The self-formed conducting filament and forming-free characteristics of as-prepared $MA_3Sb_2Br_9$ were induced by the initially formed metallic Sb and bromide vacancies. The device had a low power consumption of 117.9 fJ/μm^2 and can perform multilevel storage and various biological synaptic behaviors using voltage pulses [176]. Furthermore, Zeng *et al.* [177], Wang *et al.* [178], and Lao *et al.* [179] constructed neural networks based on lead-free HP memristors to simulate the supervised image recognition system with good accuracy. The reported devices demonstrate promising potential for combining visual information processing with machine learning, as they possess both effective optical memory and bio-inspired functionality.

In 2019, Cheng *et al.* [180] used $Cs_2AgBiBr_6$ for the first time to build memristors with long-term potentiation and depression properties under continuous pulse sequence stimulation shown in Fig. 5(d). Besides, they found that the memristors can withstand harsh conditions, as shown in Figs. 5(e, f), including high humidity, high temperature, alcohol lamp burning, and ^{60}Co γ-ray irradiation. Due to the strong Ag–Br bond and proven good crystallinity of the $Cs_2AgBiBr_6$ in the field of PSCs [180], the sandwich structure device maintained its high-end performance after more than 10^4 times bending and 10^5 cycles of reading and writing. This memristor exhibits exceptional resistance to harsh environments, surpassing that of current commercial flash memory and marking a breakthrough in the lifespan of HP memristors [181, 182].

Qian *et al.* [183] developed ITO/$MASnBr_3$/Au memristors that achieved a switching ratio of 10^3 and could withstand more than 10^4 pulse stimuli. On this basis, the multi-stage storage of information is realized. The device can store information in four different conductance states and maintain these states for more than 10^4 cycles. The time for writing and reading is 0.6 and 8 μs respectively, and the device maintains good repeatability even after being bent 1000 times, suggesting potential for flexible devices [184, 185]. In 2023, due to

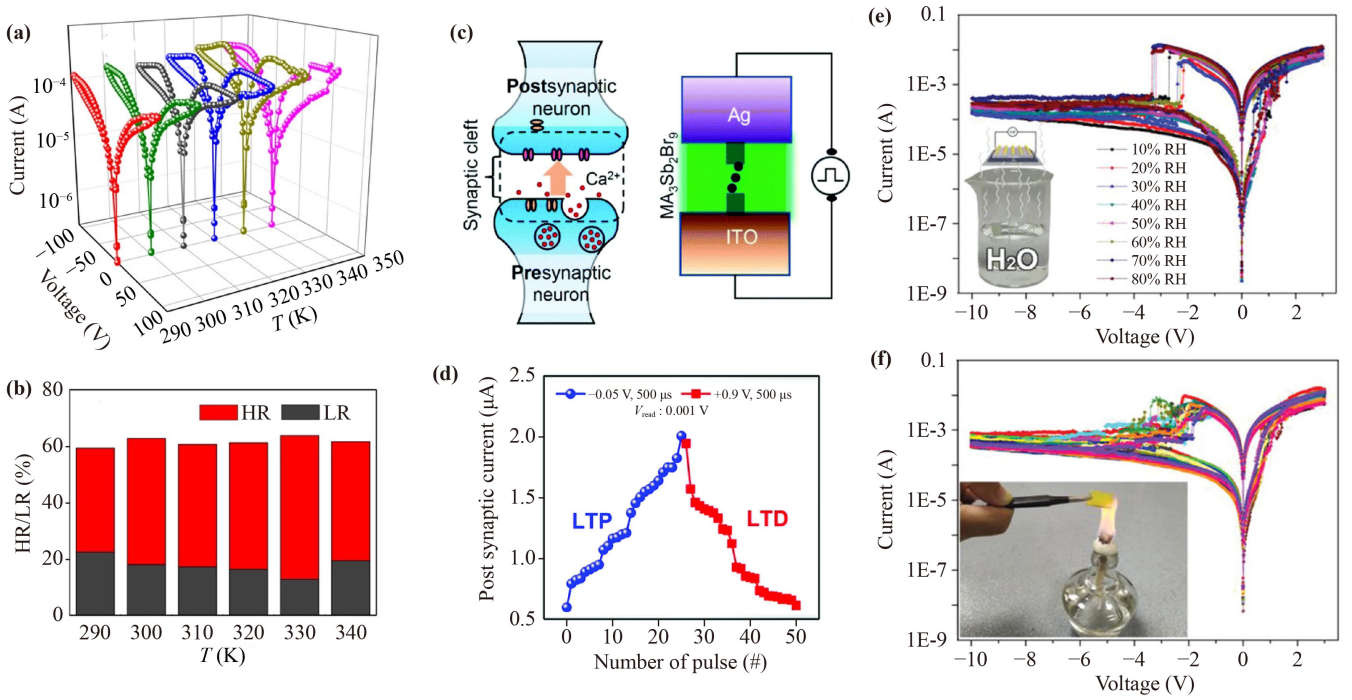

Fig. 5 **(a)** The I–V characteristics of Ag/$(CH_3NH_3)_2FeCl_4$/Cu devices measured in the temperature range from 290 K to 340 K, and **(b)** the ratio of HRS/LRS at different temperatures when the reading voltage is 0.5 V. **(c)** The biological synaptic conceptual diagram simulated by the memristor. **(d)** The long-term potentiation and long-term depression properties of the memristor under continuous pulse sequence stimulation. I–V characteristic curves of $Cs_2AgBiBr_6$-based memristor under **(e)** different humidity and **(f)** continuous alcohol lamp burning. (a, b) Reproduced from Ref. [175]. (c, d) Reproduced from Ref. [176]. (e, f) Reproduced from Ref. [181].

the unique structure of isolated octahedrons of the lead-free HPs, memristors of Al/$Cs_3Cu_2Br_5$/ITO can maintain robustness in harsh environments with humidity up to 80%, which is ideal for moisture-proof electronics [183].

In 2020, Zeng *et al.* [177] produced $Cs_3Cu_2I_5$-based perovskite with similar performance indexes such as high switching ratio, low operating voltage, and stable durability. The conductance of the device can be accurately adjusted through a series of square waveforms, and the conductance adjustment is converted into weight modulation information. It was applied to the 28 × 28 neural networks simulations, which achieved more than 94% accuracy of digital recognition from the MNIST database. This provides a promising way for the manufacture of hardware-based neural networks [177].

In conclusion, the use of lead-free and low-lead HPs-based memristors offers several advantages beyond being environmentally friendly. These advantages include a high switching ratio, low power consumption, and long lifespan, making them highly suitable for a wide range of practical applications, especially in neuromorphic computing and flash memory. However, the lower carrier mobility of lead-free HPs presents a challenge for memristors, and more research is needed in areas such as band structure engineering, forming alloys with lead HPs, and adding conduction dopants like graphene and carbon nanotubes.

4.2 Low-dimensional HP memristors

Although 3D HPs have various advantages, they are facing limitations in the pursuit of high-performance HP memristors due to high trap density, phase separation caused by photons or electrically active ions, and unstable grain boundaries with high defect density [186]. To overcome these issues, low-dimensional HPs are considered a potential solution and have recently been studied extensively. Unlike polycrystalline HPs films, low-dimensional HPs devices exhibit fewer defects and higher crystallinity due to the anisotropy and large specific surface area of single crystal structures. Moreover, the quantum confinement effect in low-dimensional HP memristors produces a special density of state (DOS) according to the dimension and can adjust the band gap according to the number of atoms. A variety of low-dimensional HPs structures including QDs [187], 1D nanowires and nanorods, and 2D layered planes have been widely reported [188–190].

4.2.1 Two-dimensional HP memristors

The distinct properties of low-dimensional HPs, such as reduced trap density, limited grain boundaries, and anisotropic electronic and optical characteristics, can enhance the performance of memristors [191, 192]. The

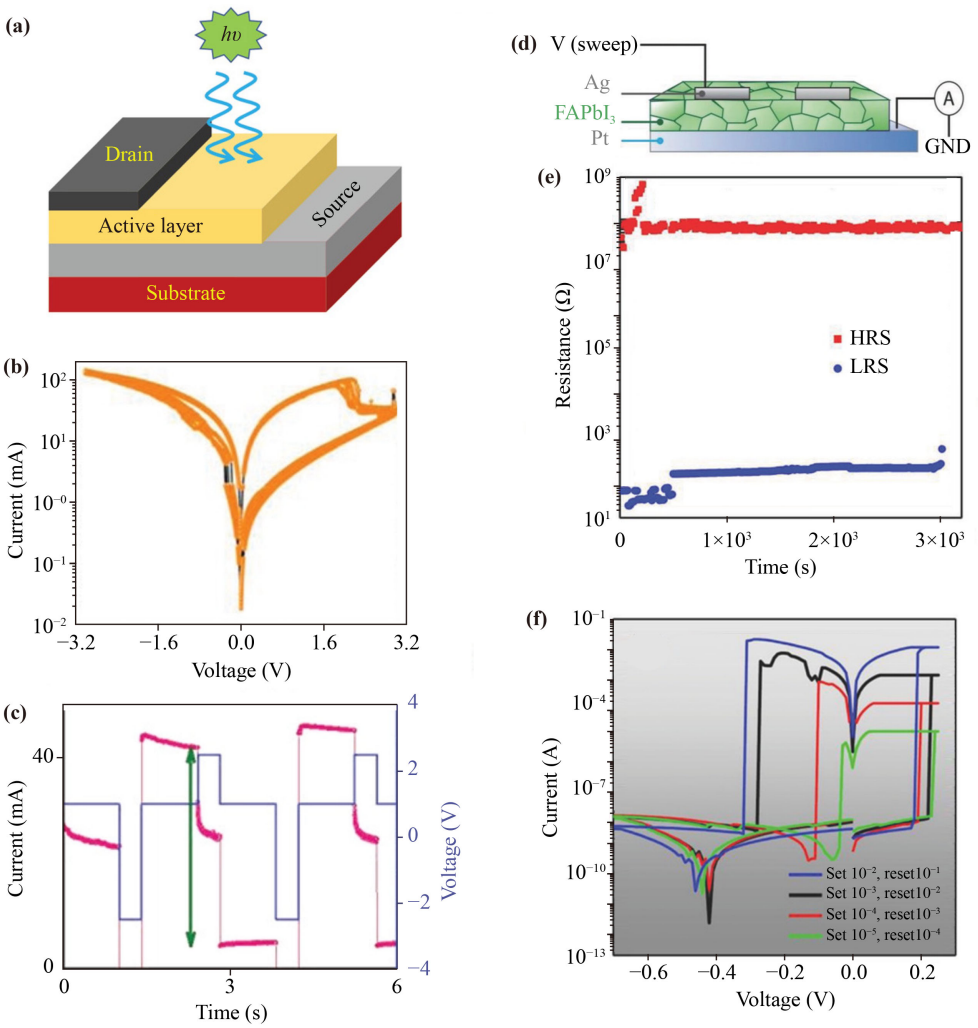

Fig. 6 **(a)** Designed device structure of simple two-terminal photodetector and the active layer is $(C_4H_9NH_3)_2PbBr_4$. **(b)** Current–voltage characteristics of the device in the dark for four consecutive cycles in a semi-logarithmic scale. **(c)** Reversible write and erasure using pulses of ± 2.5 V (read voltage is 1 V). **(d)** Schematic device structure and bias configuration of δ-$FAPbI_3$. Resistive characteristics of δ-$FAPbI_3$: **(e)** Retention time of LRS and HRS; **(f)** Multi-valued memory characteristics measured at different current levels. (a–c) Reproduced from Ref. [195]. (d–f) Reproduced from Ref. [196].

anisotropic properties can facilitate the control of filament formation and decomposition by limiting the electrical-induced movement of ions and vacancies within the intralayer of the 2D structure. The high intrinsic resistivity, which comes with lower trap density, can also improve memory performance by suppressing the OFF current. Additionally, low-dimensional HPs have better stability due to their lower hygroscopicity [193].

In 2018, Kumar *et al.* [194] used 2D HPs $(C_4H_9NH_3)_2PbBr_4$ as the active layer in memristors and the structure of the device is shown in Fig. 6(a). As shown in the following Fig. 6(b), the device represented the transition from LRS to HRS with a set voltage of 2.3 V. No abrupt change of current was observed, and it indicated that the conduction mechanism of the device can be well explained by Br ion migration induced by electric field [194]. It also displayed an optical response that can be controlled by bias voltage shown in Fig. 6(c), making it suitable for intelligent optical detection equipment [195]. The novel bilayer optoelectronic devices composed of highly transparent see-through HPs open up new opportunities for designing high-performance memristors with photosensitivity and simple architectures based on two-terminal transistors.

4.2.2 One-dimensional HP memristors

Yang *et al.* [196] compared the impact of different lattice orientations of 1D perovskite on memristors properties. With the same device structure shown in Fig. 6(d), the study found that 1D-hexagonal $FAPbI_3$ (δ-$FAPbI_3$) can show resistive switching behavior, while 3D-trigonal

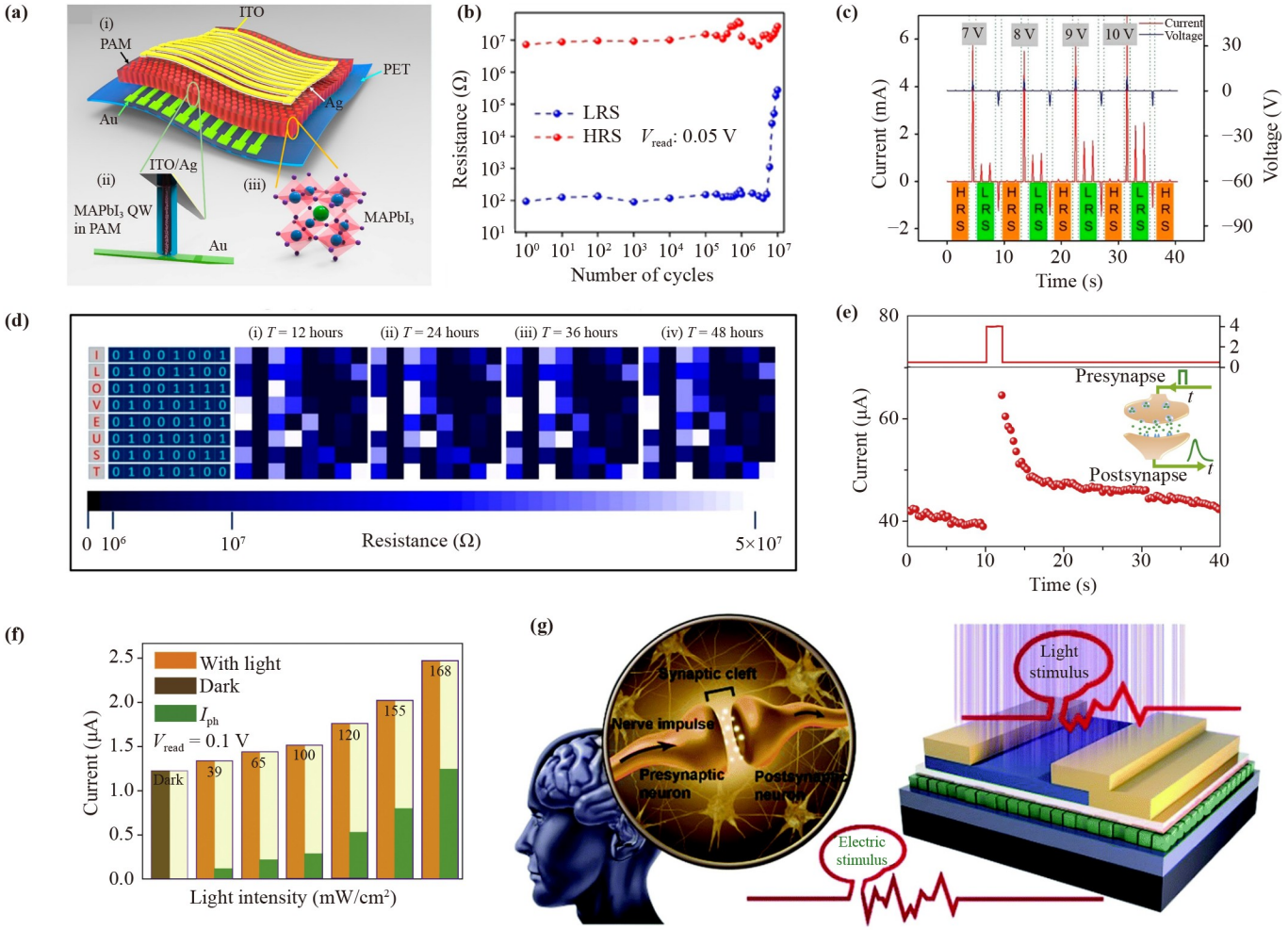

Fig. 7 **(a)** Schematic showing $MAPbI_3$ QWs memristors: (i) Device structure of ITO/Ag/MAPbI3/Au/PET; (ii) enlarged schematic of a single QW; (iii) crystal structure of $MAPbI_3$. **(b)** The durability of different resistance levels of QWs devices is studied, showing the constancy of the on/off ratio and repeatability of the system. **(c)** For different voltage pulses, multiple different LRS are displayed, and constant amplitude voltage pulses are used to read and erase. **(d)** The concept of storing data in alphabetical is illustrated matrix design order and the corresponding data time retention. **(e)** EPSCs of the device under single pulse, illustrated with a schematic diagram of the connection between EPSCs behavior and biological synapse. **(f)** The change of photocurrent of the device under different light intensity. **(g)** Structure diagram of synapses and devices. (a–d) Reproduced from Ref. [197]. (e, f) Reproduced from Ref. [199]. (g) Reproduced from Ref. [200].

$FAPbI_3$ (α-$FAPbI_3$) did not due to varying migration barriers. The effect of different annealing temperatures on the resistive switching process in memristors was also studied, and an optimal temperature of 395 K was identified to achieve symmetrical switching voltage and a high on/off ratio of 10^5 shown in Fig. 6(e). Multi-stage storage capacity was also confirmed shown in Fig. 6(f) [196]. Different structures of $FAPbI_3$ prepared at high/low temperatures exhibit significant differences in memristors, which provide valuable insights for the material design of resistive switching memory devices.

In 2021, Poddar *et al.* [197] made new progress in the application of $MAPbI_3$ quantum wires (QWs) memristors. They successfully prepared the memristor arrays on the flexible PET substrates with the structure of ITO/Ag/$MAPbI_3$/Au/PET shown in Fig. 7(a), achieving a switching ratio of 10^7 [Fig. 7(b)], an ultra-fast response of about 100 ps, and a holding time of more than two years. Through the rigorous study of the mechanism, it is proved that the switching behavior comes from the redox of Ag ions and the migration under the action of the electric field, which is consistent with the mechanism of most memristors with Ag as electrodes. The team also studied the relationship between the wire length and programming voltage, concluding that there is a threshold electric field in the device. The multi-level storage function of the device is confirmed by continuous reading, writing, and erasing. In Figs. 7(c, d), the device has four LRS and a string of letters is programmed into the memory device in the form of ASCII code. The erase voltage increased by 70% and the LRS current increased by an average of 25% under light due to the AgI generated by

the reaction of Ag with $MAPbI_3$, which decomposes under light to produce additional Ag^+ migration and improves the response current [197]. In 2023, $CH_3NH_3PbI_xCl_{3-x}$ single ultra-long nanowires were successfully synthesized and exhibited bipolar resistive switching behaviors [198]. The unique features in nanoscale exhibited by perovskite QWs memristors suggest their potential as a promising technology for next-generation nonvolatile memory with diverse applications in integrated optoelectronics and wearable devices.

4.2.3 Zero-dimensional HP memristors

In 2020, two research groups successfully fabricated artificial synapses based on monolayer $CsPbBr_3$ QDs. Chen of Tianjin University simulated various synaptic functions using optical or electrical pulses, such as photo-induced excitatory postsynaptic currents (EPSCs) behavior, short-term memory (STM), long-term memory (LTM), STM to LTM transition, and learning-forgetting-relearning behavior [Figs. 7(e, f)]. To verify the mechanical flexibility of the memristor, the device can still show slow switching behavior after 100 times bending [199]. Gong *et al.* [200] discussed the effects of electrode symmetry and wavelength of light on the memristor behaviors and fabricated a nonvolatile memristor with photon modulation and integrated synaptic plasticity customization behavior [Fig. 7(g)]. The photoelectric plasticity and memory phenomenon of both groups of research can be attributed to charge trapping and de-trapping. Similar optical programming capabilities enable the memristors in both studies to simulate synaptic plasticity under light stimulation, which provides a cost-effective direction to build artificial synapse devices with photoelectric operations in the field of memory architecture design using QDs.

Recently, reconfigurable devices which can convert between volatile and nonvolatile devices have also received extensive attention [201, 202]. And in 2022, Rohit *et al.* [203] proposed reconfigurable HP memristors, which for the first time realized the on-demand switching between diffusion/volatile and drift/nonvolatile modes while maintaining high performance. The memristor was encapsulated with oil-based guanidine bromide (OGB) ligands and achieved champion durability in both modes, as shown in Figs. 8(a, b). The author also verified the excellent performance of this circuit by calculating four different nerve pulse modes: burst, adaptation, rigidity, and irregularity, and achieved a classification accuracy of 85.1% for these four distinctive pulse sequences [Figs. 8(c, d)]. The order of priority of STM is an important part of the calculation of the reserve pool, enabling threshold switching using Ag and Br ions driven by an external electric field along the migration of NCs soft crystal lattices for diffusion mode [203]. In 2023, the incorporation of $Cs_2AgSbBr_6$ nanoparticles at different concentrations in PMMA films has been found to modulate the resistive switching behavior of memristors. It provides a simplified approach for the transition of memristors from digital to analog functionality, opening up new possibilities for reconfigurable devices [204].

In summary, Low-dimensional HPs have wider bandgap and higher stability than 3D HPs due to their reduced dimensionality and suppressed ion migration. These properties make them suitable for memristor applications requiring tunable conductance states, low power consumption, and fast response. However, low-dimensional HPs also face some challenges, such as structural complexity and carrier transport barriers. Moreover, their synthesis can be complex and time-consuming. Therefore, more research is needed to optimize their performance and overcome their limitations for memristor applications.

4.3 Multi-dimensional and heterostructured HP memristors

A semiconductor heterostructure refers to a composite arrangement consisting of two or more different semiconductor materials stacked together [205]. These structures find widespread use in various optoelectronic devices, including PSCs, LEDs, memristors, and photodetectors, among others[206]. Heterostructures exhibit distinct carrier behaviors, interactions of light and electrons, and other physical properties compared to single-component semiconductor materials. Leveraging the outstanding properties of HPs, the formation of heterostructures with other materials enables the realization of increasingly advanced device functions.

One notable category is 3D-1D HP memristors, where a 3D HP interfaces with 1D nanostructures, such as nanowires, nanotubes, or nanorods. These 1D nanostructures demonstrate unique electronic and optical properties due to quantum confinement effects. In 2021, Sun *et al.* [207] utilized a heterojunction composed of carbon nanotubes (CNTs) and HP QDs to develop an efficient neuromorphic vision system capable of information storage, processing, and light-tunable synaptic characteristics at the array level. As shown in Figs. 9(a, b), this well-designed interface between CNTs and $CsPbBr_3$ QDs enables efficient dissociation of photogenerated electron-hole pairs at the interfaces between the two materials. The integration of 1D nanostructures with 3D HPs enhances charge transport, reduces charge trapping, and improves overall memristor device performance [207].

Another type of heterostructure is the 3D–2D halide perovskite memristors, wherein the 3D HPs are combined with 2D layered materials like graphene or transition metal dichalcogenides (TMDs). These 3D HPs possess excellent charge transport properties and light-harvesting abilities, while the 2D layered materials offer

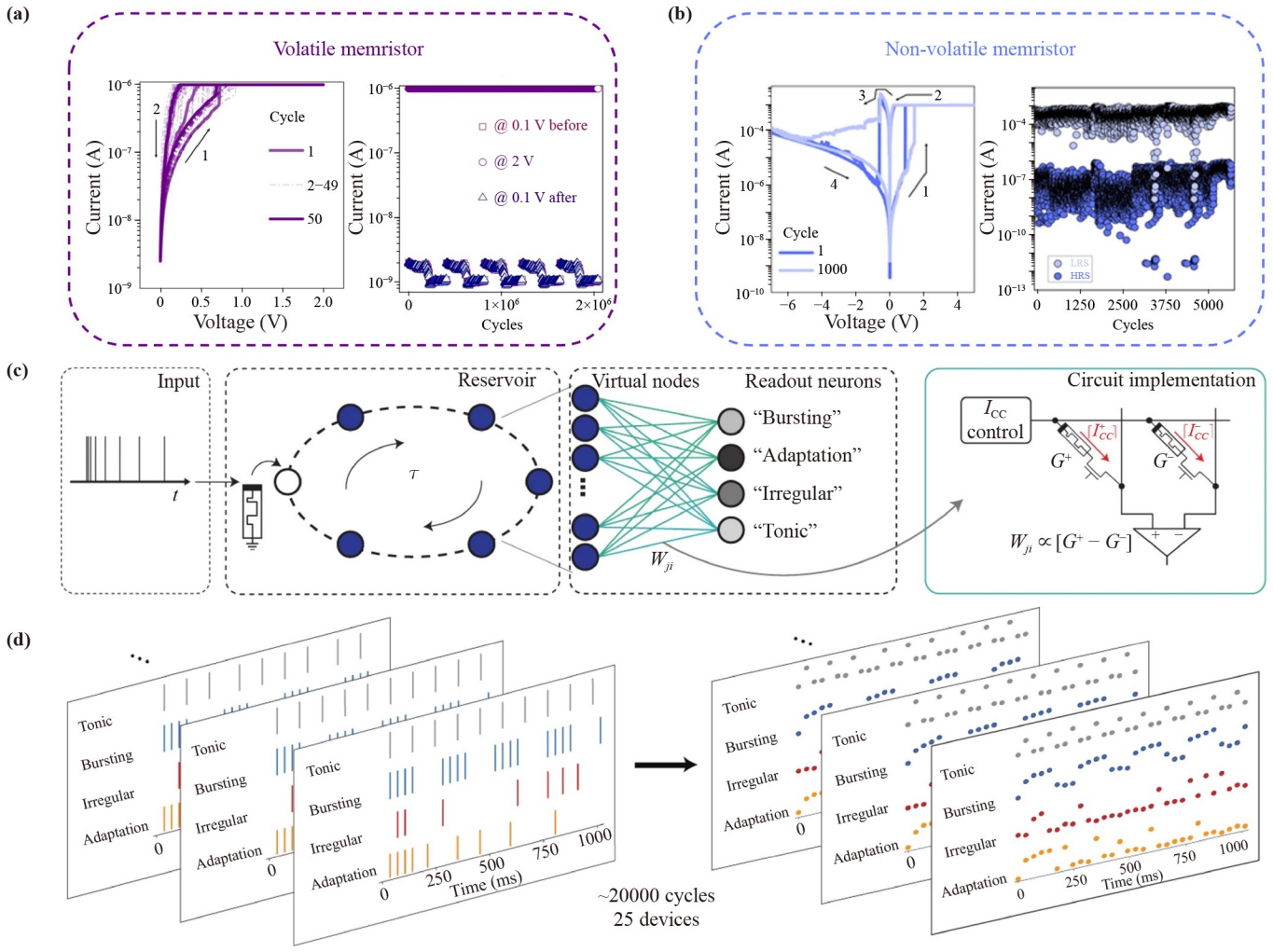

Fig. 8 **(a)** The evolution and durability of the conductance of devices as volatile devices in diffusion mode. **(b)** The evolution and durability of conductance of devices as nonvolatile devices in drift mode. **(c)** The ANN model built to demonstrate storage cell calculation; and **(d)** Four different neural discharge input modes and their resulting conductance changes in the device (voltage stimulus is 1 V, a read voltage is ±0.5 V). (a–d) Reproduced from Ref. [203].

exceptional electrical and mechanical characteristics. In a notable study by Yang *et al.* [207] in 2020, an OIHP ($MAPbI_3$) was combined with a Si nanomembrane to create a 3D–2D heterojunction. The resulting photogating effect enhanced the device's light sensitivity and achieved low energy consumption while mimicking synaptic functions, as shown in Figs. 9(c–f) [208].

Incorporating low-dimensional HP heterojunctions and hybrid interfaces will capitalize on the unique properties of each material to enhance device performance and functionality. For example, the integration of $CsPbBr_3$ memristors with ZnO [209] or PMMA [210] has shown improved charge transport and device stability. The semiconductor layer can also serve as a buffer to prevent direct contact between the HPs and metallic electrodes, reducing device degradation. Similarly, a study by Thomas *et al.* [211] demonstrated high efficiency in charge generation and transport by combining HP QDs with graphene to create G-HP QDs, as shown in Fig. 9(g). The device exhibited different response characteristics under varying gate voltages, which allowed for the building of an SNN for unsupervised machine learning and face recognition.

The exploration of multi-dimensional and multi-layer HP memristors holds promise for advanced memory devices and neuromorphic computing applications. By combining HPs with 2D, 1D nanostructures or other semiconductor materials, opportunities for enhanced device performance, energy efficiency, and novel functionalities arise. The preparation of perovskite/perovskite heterostructures is also a promising but relatively complex method that holds potential for future applications in this field [212]. However, challenges related to stability, scalability, and understanding complex switching mechanisms remain, necessitating further investigation to unlock the full potential of heterostructured HP memristors.

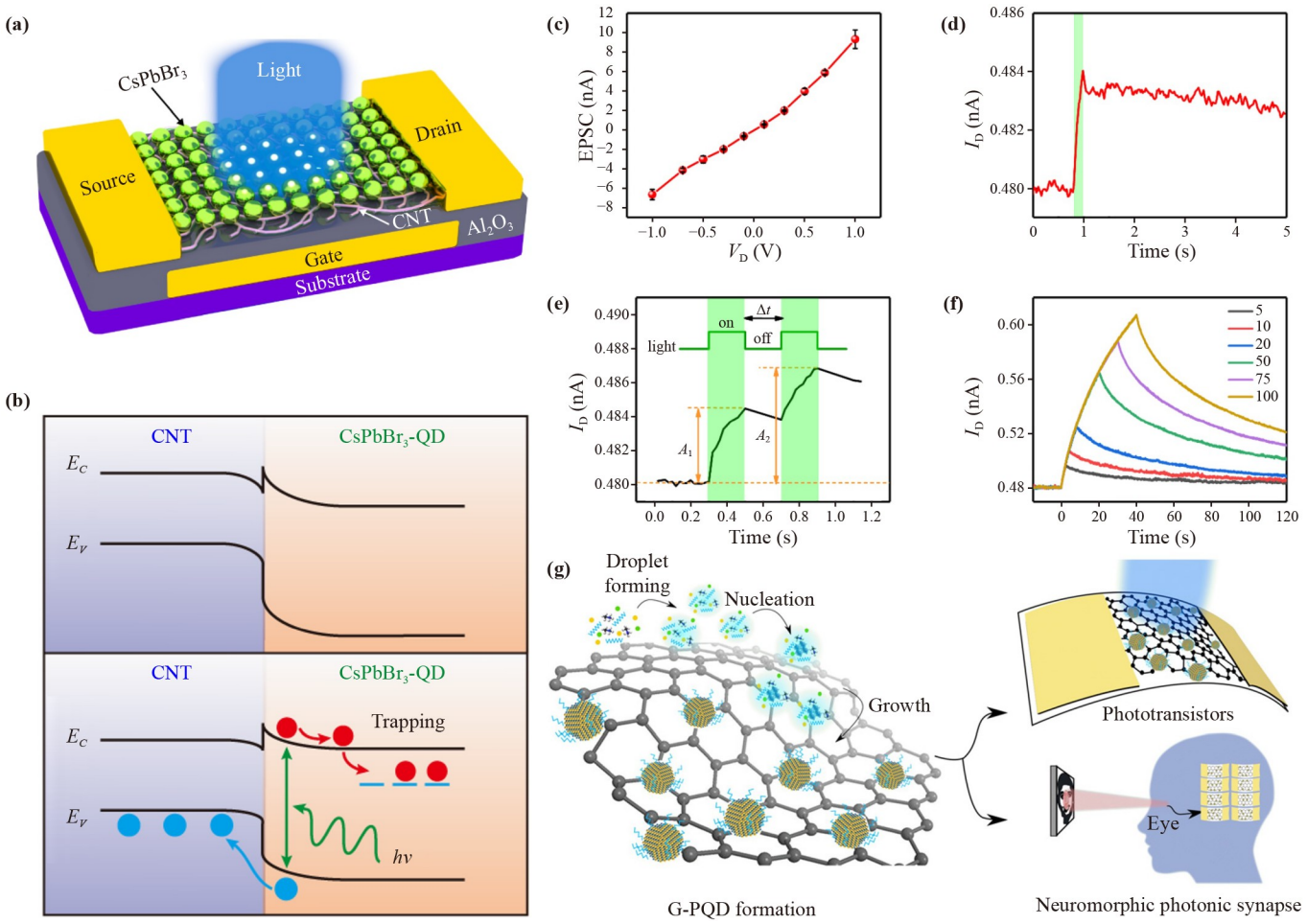

Fig. 9 **(a)** Schematic of the phototransistor with a CNTs/$CsPbBr_3$-QDs channel. **(b)** Energy band diagram at the light-off (top panel) and light-on states (bottom panel). **(c)** Dependence of the EPSC triggered by an optical spike on the source-drain voltage (V_D). **(d)** EPSC of a synaptic transistor at $V_D = 0.01$ V triggered by an optical spike. **(e)** PPF behavior of a synaptic transistor at $V_D = 0.01$ V. **(f)** Transition from STM to LTM for a synaptic transistor at $V_D = 0.01$ V with the increasing quantity of optical spikes. **(g)** Schematic showing the growth of HP QDs on graphene to form the G-HP QDs heterostructures and the proposed applications. (a, b) Reproduced from Ref. [207]. (c–f) Reproduced from Ref. [208]. (g) Reproduced from Ref. [211].

5 Applications

In the traditional information system, a traditional von Neumann architecture is often adopted. The architecture indiscriminately transmits all received data to the cloud for processing, which aggravates the computing pressure of the processor, leading to a significant amount of redundant data [213]. At the same time, it also hinders the optimization of information processing speed and energy consumption.

In the realm of overcoming the von Neumann bottleneck, HP memristors stand out as a promising innovation with diverse applications, offering solutions to the limitations of traditional information systems. One significant advantage of HP memristors is their ability to mimic the accumulation process of membrane threshold potential in biological neurons through the drifts and diffusion of movable ions. This behavior enables HP memristors to demonstrate the integrating and firing function of artificial neurons, resulting in faster and more energy-efficient data parallel processing compared to CMOS devices. Adopting HP memristors in neuromorphic computing architectures that employ ANNs for tasks like recognizing, memorizing, and creating offers potential solutions to overcome the limitations of traditional von Neumann architecture. Unlike conventional CMOS-based systems that require multiple sets of Booleans to implement essential synapse functions, memristor-based neuromorphic hardware enables a single memristor unit to serve as an individual artificial synapse [214]. This progress in architecture holds promise for enhancing computational capabilities in neuromorphic systems.

Furthermore, HP memristors offer greater flexibility when integrated into big data memory systems. Unlike

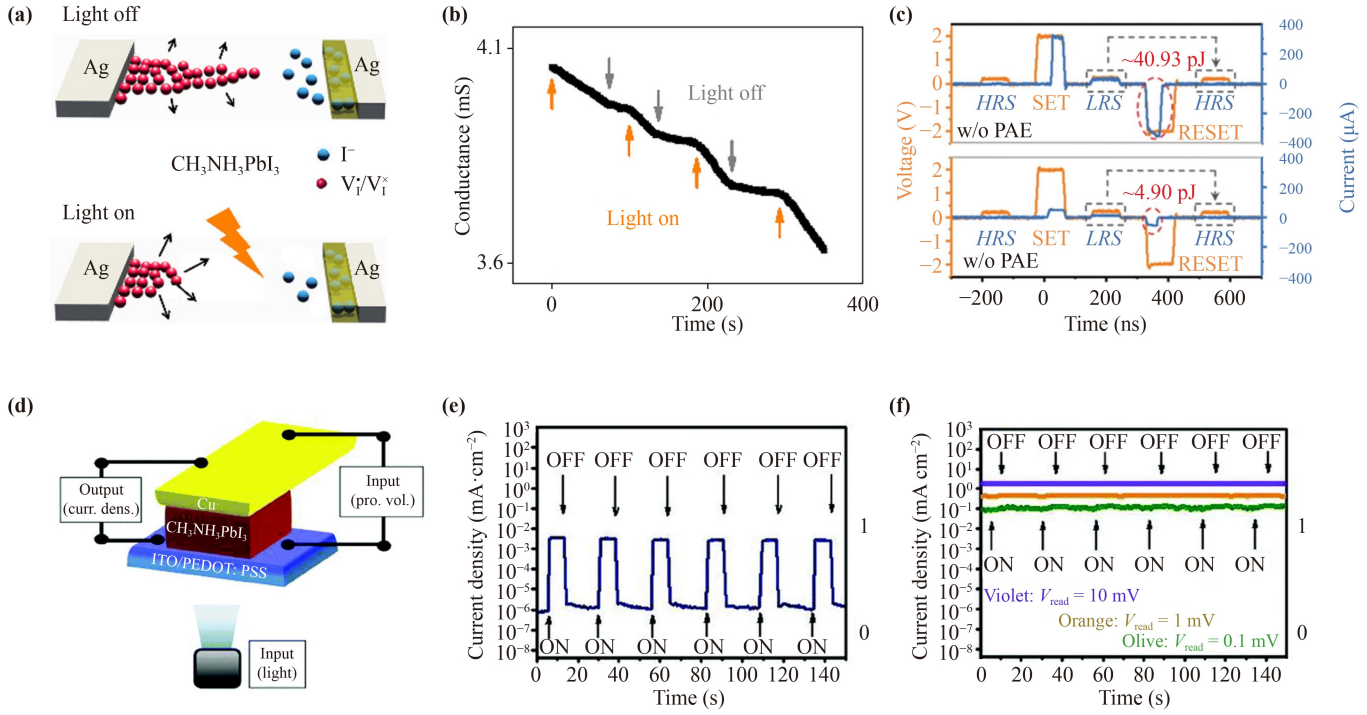

Fig. 10 **(a)** Schematic diagram of the mechanism of optically tunable synaptic behavior. **(b)** The conductive state retention of the device when the light is selectively turned on. **(c)** Current curves of memristors with and without PAE processing in pulse programming mode. **(d)** The structure diagram of the light-induced logic gate. **(e)** Light-induced switching of the device under HRS (read voltage is 10 mV). **(f)** The light-induced switch of the device under LRS (the reading voltage is 0.1, 1, and 10 mV). (a, b) Reproduced from Ref. [215]. (c) Reproduced from Ref. [216]. (d–f) Reproduced from Ref. [217].

digital devices with binary states of "0" and "1", HP memristors enhance localized data processing capabilities with their tunable multi-conductance states, providing a vast storage capacity. Through their unique properties and applications, HP memristors have the potential to optimize IoT systems by reducing the burden on the processing system and minimizing the transmission of redundant data, thereby improving the overall system performance.

5.1 Optical logic gates and non-volatile memory

One of the most promising applications of HP memristors is in photonics due to their excellent light absorption and emission properties, particularly in photovoltaic devices and optoelectronic synapses. A variety of revolutionary computing technologies, including photon memristor and photon computing, are being used to replace traditional methods. In 2018, Lu *et al.* [215] used the genetics of light to promote the progress of memristors in regulating nerve and synaptic functions [Fig. 10(a)], and the strategy of regulating Ca^+ concentration by light to simulate synaptic plasticity and its learning and forgetting behaviors at different stages of nerve development [Fig. 10(b)]. An effective method for real-time ($\leq$ 20 ms) modification of synaptic plasticity and optimization of memristor functions is proposed. Memory behaviors, including PPF, STM to LTM transition, LTM effect, learning, and forgetting, were observed on the $MAPbI_3$ memristor by controlling the wavelength and intensity of light [215]. HP memristors have the potential to offer faster switching speeds and lower energy consumption compared to other types of memristors, making them a particularly attractive option for this application.

In 2020, Zhao *et al.* [215] made perovskite memristors using light-assisted electroforming, and for the first time, proposed a simple photo-assisted electroforming (PAE) method to restrain current overshoot, which helps to restrain the performance degradation of the resistive switching process [87]. By using the PAE method, the reset current and power consumption is significantly reduced, as shown in Fig. 10(c). The authors also investigated the effects of different light intensities and wavelengths on the resistive switching behaviors of devices. They found that higher light intensities lead to lower switching voltages up to a certain threshold, while shorter wavelengths had a more significant effect on reducing the operation voltage [216]. Memristors based on HPs could potentially be used as optoelectronic switches and memory in photovoltaic devices with more efficiency and versatility.

Another potential application for HP memristors is in the field of non-volatile memory. Non-volatile memory is

used to store data even when power is turned off and has a wide range of applications in electronic devices such as computers, mobile phones, and wearable devices. In 2015, Lin *et al.* [215] used OIHP materials as building blocks of non-volatile memristors. Devices with structures of ITO/PEDOT: PSS/$MAPbI_3$/Cu show obvious characteristics of electrical stability and non-volatile rewritable memory effects. By applying the voltage scanning of 0 V→ –3 V→3 V→0 V, fitting data of characteristic curve can be divided into ohmic conduction region and FPE region. They believe that the mechanism of the device is the interlayer barrier, in which charge transfer was caused by trap-controlled SCLC processes. In addition, they also found the light response characteristics of $CH_3NH_3PbI_3$. Based on this, the OR gates of optical and electrical inputs can be constructed [Fig. 10(d)], and the current levels can be used as outputs. As shown in Fig. 10(e), under simulated sunlight (100 mW/cm^2), the device responds significantly to light only in the HRS state, and it cannot be turned on or off by selecting a different read voltage in LRS [Fig. 10(f)]. The information flow can be further realized by additional current-to-voltage converters, which help to realize logic gate operations at the hardware level [217]. HP memristors have demonstrated excellent stability and long data retention times, making them an attractive option for non-volatile memory applications.

In 2020, Xing *et al.* [215] reported the latest progress of $MAPbBr_3$ single crystals [Fig. 11(a)], and fabricated the memristor based on a single crystal block for the first time, showing adjustable conductances and stable switching effects. Polarization is carried out by applying voltage bias, and a voltage of 20 V is selected to adjust the defects. In this study, the conduction voltage was maintained at ~0.4 V due to the larger ion transport energy in the single crystal, so the J–V hysteresis loop in Fig. 11(b) was mainly attributed to the charge capture and de-trapping mechanism. Under a reading voltage of 1 V, the Au/$MAPbBr_3$/Au device shows stable multi-conductance states by adjusting different biases, as shown in Fig. 11(c) [218]. It has the potential to realize the multi-stage storage function of the basic memristor.

5.2 Artificial synapses and neural networks

HP memristors also have the potential to be used in neuromorphic computing. In this field, the memristors can mimic the synaptic behaviors of biological neurons, allowing for the creation of ANNs [219]. In organic organisms, using electrical or chemical signals as the transmission media of biological synapses can achieve a very low power consumption and fast processing speed [220, 221]. This is mainly due to the large number of synapses and the advanced function of nerve cells. Therefore, brain-like and bionic synaptic devices are becoming the focus of scientific and industrial attention because of their low power consumption, small size, and high speed [222, 223]. Zhang's group [224] utilized air-stable $CsCu_2I_3$ perovskite thin films to fabricate artificial synapses and demonstrated their high accuracy in neuromorphic computing in MNIST database recognition. They also provided an adequate explanation for the emergence mechanism of synaptic behaviour in two-dimensional perovskite thin films through density functional theory (DFT) calculations [192]. By uncovering the underlying principles of perovskites and showcasing their applicability in neuromorphic computing, the research lays the foundation for further advancements in the field.

In 2020, Zhu *et al.* [225] proposed a reservoir computing (RC) system based on $CsPbI_3$ memristors shown in Fig. 11(d). The HP memristors can be driven by simulated nerve spikes, with the state of the memristor reflecting the time characteristics of the nerve spikes. The RC system relies on STM, which means that the reservoir state depends on the input of the recent past in addition to the present input. The Ag/$CsPbI_3$/Ag reserve pool is evaluated in terms of internal dynamics, nonlinearity, fading memory, separability, and echo state characteristics, and applied to the analysis of real-time neuron interactions. The results show that these devices can be potentially driven by actual biological nerve spikes and interface with nerve probes for nerve discharge pattern recognition and nerve synchronization analysis [225].

In the same year, Huang *et al.* [225] fabricated a zero-power photoelectric synaptic device based on a mixed structure of Si NCs and HPs. The device successfully simulated synaptic plasticity such as PPF, spike-rate dependent plasticity (SRDP), and spike-number dependent plasticity (SNDP). By specifying the frequency of the filter, the device sharpens the pattern by passing signals whose frequency is higher than f_H through the filter and attenuating signals whose frequency is lower than f_H, as shown in Figs. 11(e–h). Based on the number of applied pulses, a corresponding relationship between numerical values and EPSC pulse numbers could be established, enabling the mimicking of arithmetic calculations in analog neuromorphic computing. The arithmetic functions of addition, subtraction, multiplication, and division using EPSCs pulse numbers as numerical values have been successfully simulated [226].

In 2022, Rohit *et al.* [225] made new progress in the task of simulating high-order synaptic devices. They demonstrated the second-order switching dynamics using the ion-electron conductivity of $MAPbI_3$. In traditional synaptic devices, the simulation of plasticity is mainly based on the facilitation of single pulses or paired pulses (such as PPF and spike-timing dependent plasticity (STDP)). This Hebbian learning rule brings some limitations and cannot fully show the impact of spike timing series and the history of synaptic activity on biological synapses. This issue is exemplified by inconsistent

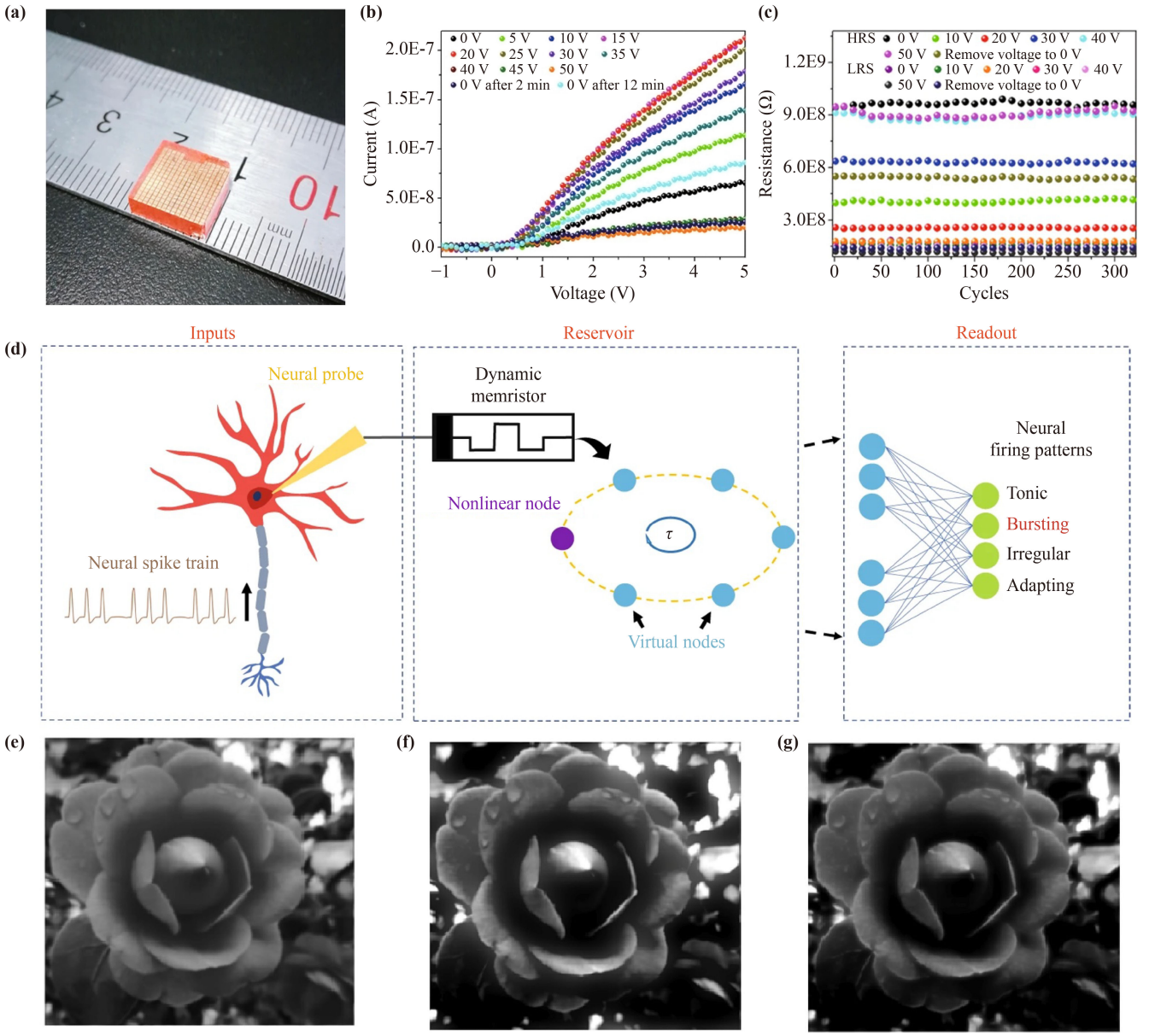

Fig. 11 **(a)** Optical photographs of centimeter-sized $MAPbBr_3$ single crystal blocks with gold electrodes deposited. **(b)** *J*–*V* characteristic curves of the device. **(c)** Various resistance states of the device under different bias stimuli. **(d)** Schematic diagrams of input, reservoir, and readout for the classification of different pulse sequences. **(e)** Original images of flowers. **(f)** The sharpened flower image through the filter when the cutoff frequency is 4.8 Hz. **(g)** The sharpened flower image through the filter when the cutoff frequency is 19 Hz. (a) Reproduced from Ref. [218]. (b–d) Reproduced from Ref. [225]. (e–g) Reproduced from Ref. [226].

results in response to the same frequency input. To address this, the authors applied the Bienenstock–Cooper–Munro (BCM) learning rule using mixed ion-electron conductivity of HPs and the triplet spike sequence dependent plasticity (TSTDP) scheme, which considers the variable third factor interacting with paired pulses. The BCM rule was applied to the mammalian binocular vision system using a feedforward neural network (FNN) simulated by taking advantage of the physical properties of HPs. Using light bars from eight different angles as inputs, the same output from the left and right eyes can always win the final choice of the network in the absence of winner-take-all and back-propagation as shown in Figs. 12(a, b). The devices' timing/frequency processing characteristics make it possible to develop a completely unsupervised system. The authors demonstrated the BCM mechanism in maximizing the response of synapses to specific inputs after receiving stimuli [227].

Overall, the field of HP memristors is witnessing a growing trend toward exploring the applications of bio-

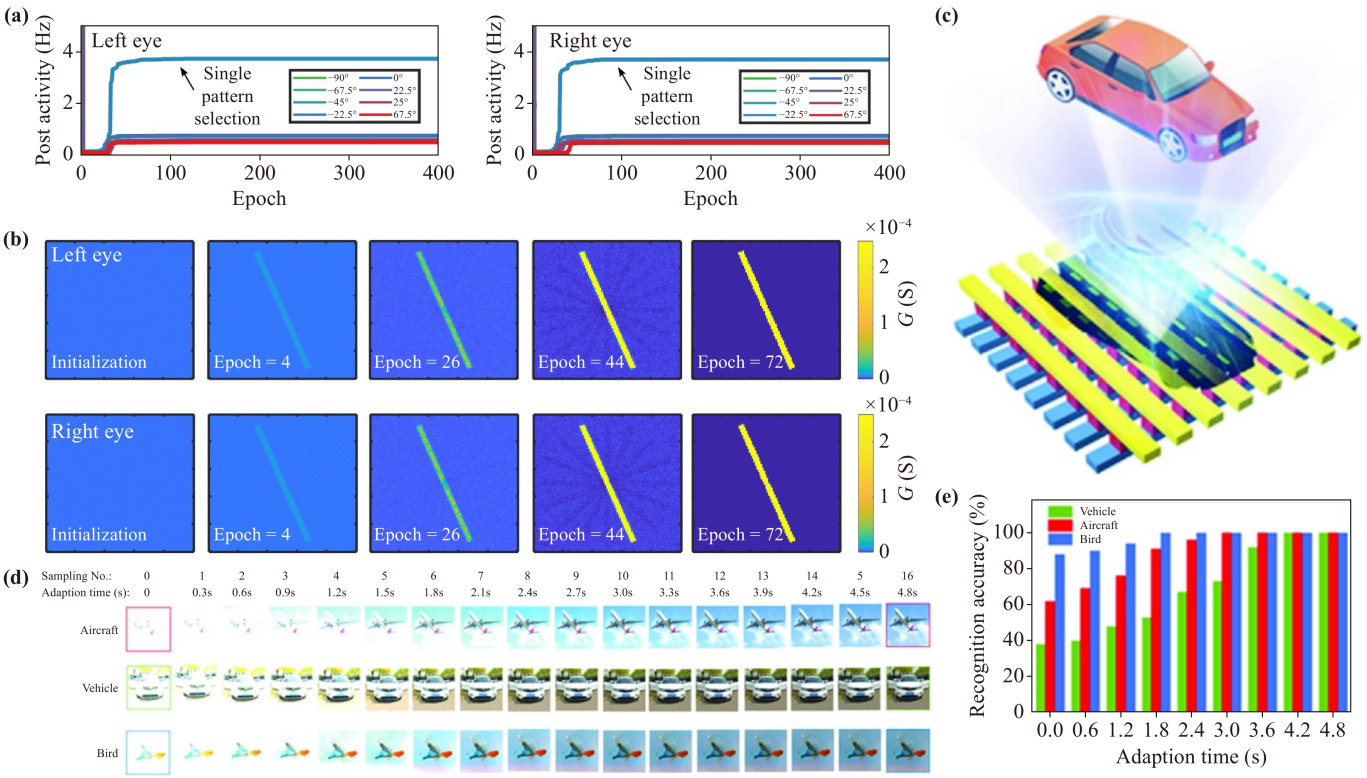

Fig. 12 **(a)** The postsynaptic activity is caused by network exposure to specific input patterns. After some epochs, the postsynaptic activity became higher for the selected mode (–22.5°), and the choice of the left and right eyes was the same. **(b)** The time evolution of the synaptic weight of the left eye and the right eye: the selectivity increased significantly after continuous exposure to the input mode after the random weight matrix was initialized. **(c)** The device structure of the CsFAMA photovoltaic sensor and the schematic diagram of the crossbar array. **(d)** The adaptive dynamic process of the overexposed image. **(e)** The recognition accuracy of the car with the door open, aircraft and bird images increase with the increase of adaptation time. (a, b) Reproduced from Ref. [227]. (c–e) Reproduced from Ref. [231].

inspired synaptic devices. This research direction holds significant promise for driving advancements in post-Moore device design and integration, big data revolution, perceptual computing, and other fields [228–230]. By drawing inspiration from the principles of biological synapses, HP memristors offer unique opportunities for pushing the boundaries of current technologies and shaping the future of computing.

5.3 Retinomorphic computing

HPs materials possess unique optical responses and certificated excellent performance in PSCs. Thus, HP memristor-based systems are capable of processing complex information similar to human visual systems, including image perception and preprocessing, as well as recognition and memory of images in the visual receptive area of the brain. HP memristor-based intelligent retinal sensing system can be used in high-density and low-power neural networks, and may also contribute to the development of humanoid sensory electronics in the next generation of robots and IoT.

In 2020, Chen *et al.* [225] demonstrated a switchable visual sensor based on CsFAMA perovskite shown in Fig. 12(c). This device is designed to simulate the adaptive process of human eyes to light intensity and enables image contrast enhancement. Probabilistic Neural Networks (PNN) were used to achieve a higher recognition and classification accuracy. CsFAMA thin films have wide band absorption covering almost the whole visible spectrum of solar radiation, which lays a foundation for RGB imaging of human eyes. The adaptive function of the device is attributed to photogenerated carriers and voltage-induced ion migration, which has been confirmed by photo-induced force microscopy (PiFM) technology. The TensorFlow framework for machine vision utilized optical illumination intensity as input, optical response as variable weight, and photocurrent as output. Taking the case of overexposure into account, as shown in Figs. 12(d, e), the photocurrent of spontaneous relaxation of ion migration induced by photovoltaic field in CsFAMA devices is very similar to the adaptive behavior of image sensing in the biological vision system, and the recognition accuracy is improved by 263% under complex lighting environment [231].

In 2020, Yang *et al.* [225] designed a self-powered artificial

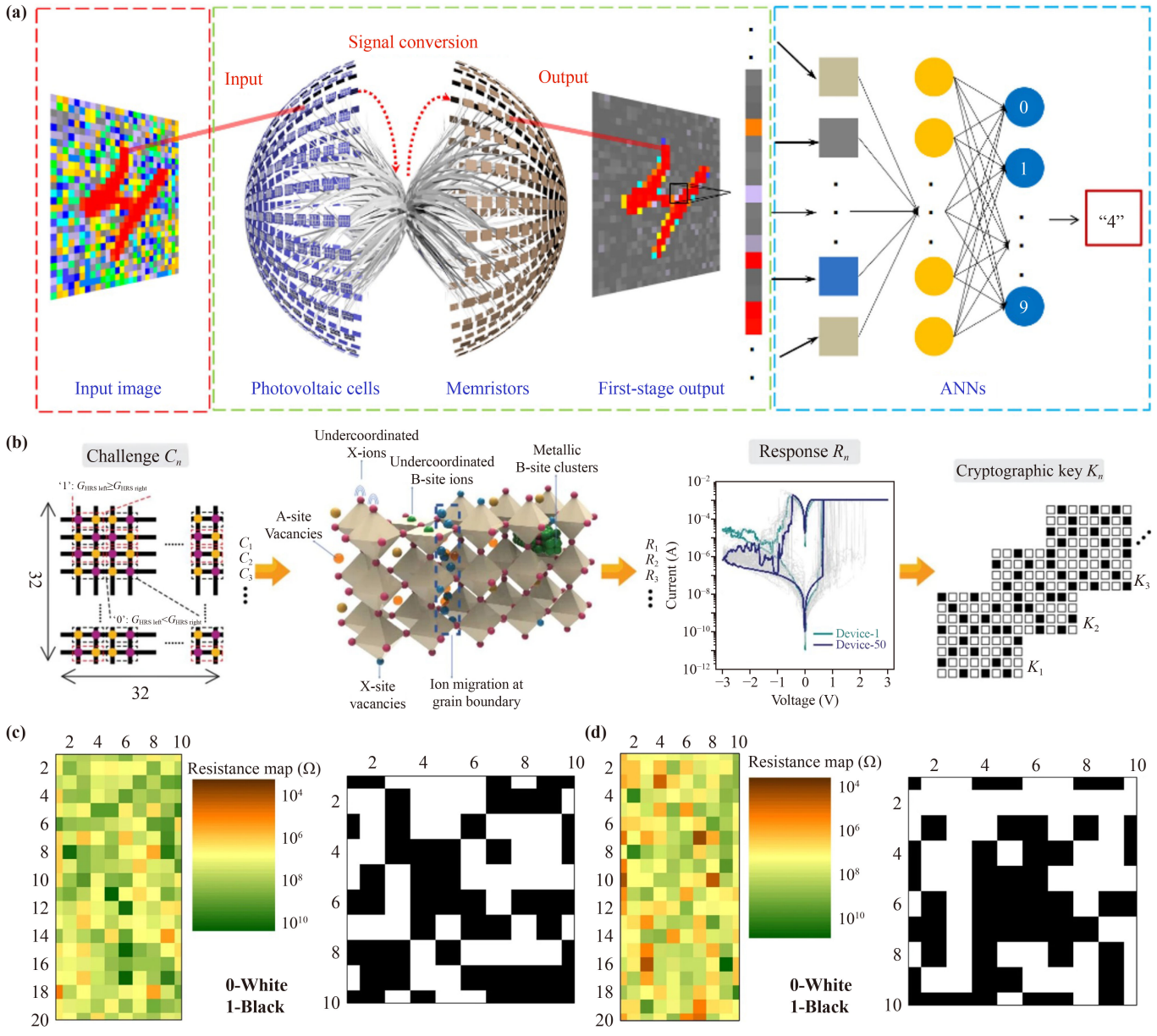

Fig. 13 **(a)** Schematic diagram of the recognition results of the self-powered artificial retina system and ANNs. **(b)** The charge transfer characteristics of HPs can be used as the source of entropy for designing a new type of PUFs. The coexistence of many kinds of switching physics in HPs makes the resistance states highly random, and the encryption key is generated from the difference of the HRS of these memories. **(c)** Before a cycle of reconstruction. **(d)** After a cycle of reconstruction, analog-digital maps and digital maps show different results. (a) Reproduced from Ref. [232]. (b–d) Reproduced from Ref. [233].

retinal sensing system composed of solar cells and perovskite-based memristors. The system consists of high-density and low-power neural networks with cross-array hardware, as shown in Fig. 13(a). The authors used passivated HP memristors with history-related conductance and reliable state maintenance capabilities to simulate the learning and memory functions of the human brain. The passivated memristor is connected to the solar cell, and the photovoltaic action drove the cell to produce a positive voltage that simulated HP memristors. The researchers also studied the effects of irradiation time, frequency, intensity, as well as wavelength-dependent plasticity of artificial optical synapses on image preprocessing.

Based on the radiation intensity-dependent plasticity, the system could enhance image memory with enhanced contrast and feature extraction in convolutional neural networks (CNNs). Image preprocessing with distinguishing irradiation wavelength can simulate the color resolution of human eyes, reduce the interference of other colors to

the image, and achieve a better noise reduction effect. Overall, the self-powered artificial retina system improved the recognition rate and reduced energy consumption at the hardware level. The proposed system is expected to be introduced to detecting and preprocessing environmental conditions for human-like sensory electronics in the next generation of robots [232].

5.4 Physical unclonable functions

Physical unclonable functions (PUFs) is a hardware security technology that uses inherent device changes to produce a unique device response that cannot be cloned. similar to human biometrics, PUFs are the inherent and unique identifiers of each chip, making them a promising technology to further improve the safety of electronic products in the future, as shown in Fig. 13(b).

In 2021, John *et al.* [225] proposed an attractive and inexpensive alternative for designing efficient encryption hardware using OIHPs ($PrPyr[PbI_3]$). The authors tested 50 devices, showing a switch ratio of 10^5, which improves the reliability of PUF. By using HRS as the entropy source of PUF design, the PUF generated a unique key of the device by converting the random analog conductance value into binary digits. For the first time, the authors reported a 1024-element array can control the bit error rate under unwanted time, voltage, and temperature fluctuations. Furthermore, they used write-back measures to ensure a reliable PUF, and the bit error rate of the regenerated response bits after write-back is 0%.

The authors also demonstrated that reconfiguring PUF keys can support ownership changes, permission changes, or prevent information disclosure due to overuse. By leveraging the memory computing capabilities of crossovers, as shown in Figs. 13(c, d), the proposed PUF construction scheme can protect PUF from modelling attacks without the need for additional cross-bars. The quality of the random bit stream generated by the device is comparable to or even better than before, with an average uniformity of 512 bits at 49.02%. The work shows that OIHP can be an effective and reliable material for designing PUFs, paving the way for further research in this area [233].

6 Outlook and challenge

In this paper, we review the latest trend of systematic research based on HP memristors and briefly introduce the materials, mechanisms, performance, and applications of HP memristors. Compared with other materials, HPs have unique electrical and optical properties, including excellent optical absorption efficiency, high charge mobility, and long charge lifetime [234]. This provides a guarantee for the multi-level modulation of HP memristors and shows great potential in the further development of neuromorphic computing. HPs have successfully been utilized in photovoltaic applications, while steady progress is being made in other photonic electronic applications such as detectors and memristors. HPs exhibit hysteresis in I–V characteristics due to the migration of ions or defects, which is suitable for the application of memristors. HP memristors can be reduced to a characteristic size of less than 2 μm, maintaining a storage state of more than 10^5 s and a nanosecond time scale switching. These characteristics are significant for realizing various functions, which is why extensive research has been done on HP memristors in the past few years.

The unique characteristics of HP memristors make them suitable for applications such as logic switches, non-volatile memory, bio-inspired computing, and intelligent retinal recognition systems [235]. HP memristors with simple device structures provide an alternative to the components of traditional silicon circuits using von Neumann architecture. The HP memristors also have the advantages of low manufacturing cost and low energy consumption.

Research on the key challenges should be strengthened to further promote its practical application of HP memristors. Specifically, materials should be considered in terms of their performance and environmental impact. Unlike PSCs, which rely heavily on Pb elements for their excellent performance, the performance of HP memristors is relatively unaffected by the replacement of B-site elements. Therefore, component engineering in HPs should be considered in future research. Additionally, the stability of low-dimensional HPs needs to be improved, requiring further exploration of perovskite packaging technology and passivation engineering to achieve long-term device stability [236].

Miniaturization of HP memristors should also be paid attention to, as the final performance of the HP memristors is highly dependent on perovskite film quality. Current methods, such as spin coating, will inevitably produce holes and uneven grains that hinder miniaturization [237, 238]. The use of anti-solvent and multi-step spin coating will improve the above situation to some extent [239], but the final solution to this problem may require the development of more novel HPs growth methods to obtain highly dense, smooth, and uniform HPs films, such as physical and chemical vapor deposition. Bolink's group has made advancements in the multi-source preparation of multi-cation HPs, resulting in improved power conversion efficiency (PCE) and stability of solar cells based on this material [240]. In the field of LEDs, the difficulties of obtaining dense and compact crystalline films through solution methods have been overcome by Bulović's group [241], who achieved uniform crystalline $CsPbBr_3$ films with complete surface coverage through vapor co-evaporation of CsBr and $PbBr_2$ precursors. As

demonstrated in these studies, precise control over the morphology of HPs films leads to reduced defects and improved charge collection, which highlights the effectiveness of vapor deposition techniques in enhancing device efficiency and stability.

Furthermore, the integration of HPs layers with the CMOS process, utilizing protective layers or other methods, is a crucial step in advancing the large-scale commercial production of HP memristors. Achieving the desired device architecture requires precise deposition techniques like photolithography or printing methods. However, the compatibility of these patterning techniques with HPs and their seamless integration into the device manufacturing process poses significant challenges. Zhang *et al.* [242] have demonstrated a potential solution by using electron beam lithography (EBL) and inductively coupled plasma (ICP) etching to pattern HPs single crystals, covering them with PMMA. This approach holds promise for the fabrication of microscale and nanoscale perovskite structures, which can be extended to the field of HP memristors preparation. The successful implementation of high-quality, uniform, and reproducible patterning techniques for HP memristors is a complex task. Overcoming this challenge facilitates the commercialization of HP memristors and may unlock their full potential in next-generation electronics and computing applications.

In terms of application, a series of new optoelectronic devices based on HP memristors have been designed and implemented. The combination of resistive switching and optoelectronic properties will broaden the application range of HPs, such as photoelectric synapses and intelligent vision systems [243]. In the field of neuromorphic devices, HP memristors have been successfully combined with various neural networks (such as CNNs, recurrent neural networks (RNNs), and deep neural networks (DNNs)), but research based on SNN is still in the early stages. However, most of the applications are still in the conceptual stage at present. Research on the relationship between the structure and function of neuromorphic devices and the synaptic mechanism based on HPs is necessary to reduce device deviation and improve storage performance.

In a word, HP memristors are showing promising prospects for various applications, and research on system-level integration will continue to progress. HPs are proving their influence in future information electronic devices through their excellent performance in a variety of applications, but further research is needed to address key challenges and improve device performance.

Declarations The authors declare that they have no competing interests and there are no conflicts.

Acknowledgements This work was financially supported by the National Natural Science Foundation of China (Grant Nos. 61974090, 62111540271, and 62104267) and the National Key R&D Program of China (Grant No. 2022YFB4700102).

References

1. Z. Xiao and J. Huang, Energy-efficient hybrid perovskite memristors and synaptic devices, *Adv. Electron. Mater.* 2(7), 1600100 (2016)
2. B. Zhang, W. Chen, J. Zeng, F. Fan, J. Gu, X. Chen, L. Yan, G. Xie, S. Liu, Q. Yan, S. J. Baik, Z. G. Zhang, W. Chen, J. Hou, M. E. El-Khouly, Z. Zhang, G. Liu, and Y. Chen, 90% yield production of polymer nano-memristor for in-memory computing, *Nat. Commun.* 12(1), 1984 (2021)
3. L. Du, Z. Wang, and G. Zhao, Novel intelligent devices: Two-dimensional materials based memristors, *Front. Phys.* 17(2), 23602 (2022)
4. Q. Li, T. Li, Y. Zhang, Y. Yu, Z. Chen, L. Jin, Y. Li, Y. Yang, H. Zhao, J. Li, and J. Yao, Nonvolatile photoelectric memory with $CsPbBr_3$ quantum dots embedded in poly(methyl methacrylate) as charge trapping layer, *Org. Electron.* 77, 105461 (2020)
5. Z. Hao, H. Wang, S. Jiang, J. Qian, X. Xu, Y. Li, M. Pei, B. Zhang, J. Guo, H. Zhao, J. Chen, Y. Tong, J. Wang, X. Wang, Y. Shi, and Y. Li, Retina-inspired self-powered artificial optoelectronic synapses with selective detection in organic asymmetric heterojunctions, *Adv. Sci. (Weinh.)* 9(7), 2103494 (2022)
6. T. Y. Wang, J. L. Meng, Z. Y. He, L. Chen, H. Zhu, Q. Q. Sun, S. J. Ding, P. Zhou, and D. W. Zhang, Ultralow power wearable heterosynapse with photoelectric synergistic modulation, *Adv. Sci. (Weinh.)* 7(8), 1903480 (2020)
7. N. El-Atab, Memsor: Emergence of the in-memory sensing technology for the digital transformation, *physica status solidi (a)* 219(2), 2100528 (2022)
8. J. C. Gonzalez-Rosillo, S. Catalano, I. Maggio-Aprile, M. Gibert, X. Obradors, A. Palau, and T. Puig, Nanoscale correlations between metal–insulator transition and resistive switching effect in metallic perovskite oxides, *Small* 16(23), 2001307 (2020)
9. Y. Li, J. Chu, W. Duan, G. Cai, X. Fan, X. Wang, G. Wang, and Y. Pei, Analog and digital bipolar resistive switching in solution-combustion-processed NiO memristor, *ACS Appl. Mater. Interfaces* 10(29), 24598 (2018)
10. J. Rao, Z. Fan, L. Hong, S. Cheng, Q. Huang, J. Zhao, X. Xiang, E. J. Guo, H. Guo, Z. Hou, Y. Chen, X. Lu, G. Zhou, X. Gao, and J. M. Liu, An electroforming-free, analog interface-type memristor based on a $SrFeO_x$ epitaxial heterojunction for neuromorphic computing, *Mater. Today Phys.* 18, 100392 (2021)
11. H. Guan, J. Sha, Z. Zhang, Y. Xiong, X. Dong, H. Bao, K. Sun, S. Wang, and Y. Wang, Optical and oxide modification of CsFAMAPbIBr memristor achieving low power consumption, *J. Alloys Compd.* 891, 162096 (2022)
12. G. Abbas, M. Hassan, Q. Khan, H. Wang, G. Zhou, M. Zubair, X. Xu, and Z. Peng, A low power-consumption and transient nonvolatile memory based on highly

dense all-inorganic perovskite films, *Adv. Electron. Mater.* 8(9), 2101412 (2022)
13. M. Lanza, A. Sebastian, W. D. Lu, M. Le Gallo, M. F. Chang, D. Akinwande, F. M. Puglisi, H. N. Alshareef, M. Liu, and J. B. Roldan, Memristive technologies for data storage, computation, encryption, and radio-frequency communication, *Science* 376(6597), eabj9979 (2022)
14. X. Yan, Q. Zhao, A. P. Chen, J. Zhao, Z. Zhou, J. Wang, H. Wang, L. Zhang, X. Li, Z. Xiao, K. Wang, C. Qin, G. Wang, Y. Pei, H. Li, D. Ren, J. Chen, and Q. Liu, Vacancy-induced synaptic behavior in 2D WS_2 nanosheet-based memristor for low-power neuromorphic computing, *Small* 15(24), 1901423 (2019)
15. J. M. Yang, J. H. Lee, Y. K. Jung, S. Y. Kim, J. H. Kim, S. G. Kim, J. H. Kim, S. Seo, D. A. Park, J. W. Lee, A. Walsh, J. H. Park, and N. G. Park, Mixed-dimensional formamidinium bismuth iodides featuring in-situ formed type-I band structure for convolution neural networks, *Adv. Sci. (Weinh.)* 9(14), 2200168 (2022)
16. X. Xiao, J. Hu, S. Tang, K. Yan, B. Gao, H. Chen, and D. Zou, Recent advances in halide perovskite memristors: Materials, structures, mechanisms, and applications, *Adv. Mater. Technol.* 5(6), 1900914 (2020)
17. Z. B. Yan and J. M. Liu, Resistance switching memory in perovskite oxides, *Ann. Phys.* 358, 206 (2015)
18. K. Kang, W. Hu, and X. Tang, Halide perovskites for resistive switching memory, *J. Phys. Chem. Lett.* 12(48), 11673 (2021)
19. S. Majumdar, B. Chen, Q. H. Qin, H. S. Majumdar, and S. Van Dijken, Electrode dependence of tunneling electroresistance and switching stability in organic ferroelectric P(VDF-TrFE)-based tunnel junctions, *Adv. Funct. Mater.* 28(15), 1703273 (2018)
20. G. K. Johnsen, An introduction to the memristor – a valuable circuit element in bioelectricity and bioimpedance, *J. Electr. Bioimpedance* 3(1), 20 (2012)
21. L. Spaziani and L. Lu, Silicon, GaN and SiC: There's room for all: An application space overview of device considerations, in: *2018 IEEE 30th International Symposium on Power Semiconductor Devices and ICs (ISPSD)*, 13–17 May, 2018, pp 8–11
22. Y. N. Zhong, T. Wang, X. Gao, J. L. Xu, and S. D. Wang, Synapse-like organic thin film memristors, *Adv. Funct. Mater.* 28(22), 1800854 (2018)
23. Y. Hao, Gallium oxide: Promise to provide more efficient life, *J. Semicond.* 40(1), 010301 (2019)
24. N. A. Tulina, I. Y. Borisenko, and V. V. Sirotkin, Reproducible resistive switching effect for memory applications in heterocontacts based on strongly correlated electron systems, *Phys. Lett. A* 372(44), 6681 (2008)
25. W. I. Park, J. M. Yoon, M. Park, J. Lee, S. K. Kim, J. W. Jeong, K. Kim, H. Y. Jeong, S. Jeon, K. S. No, J. Y. Lee, and Y. S. Jung, Self-assembly-induced formation of high-density silicon oxide memristor nanostructures on graphene and metal electrodes, *Nano Lett.* 12(3), 1235 (2012)
26. Z. Ma, J. Ge, W. Chen, X. Cao, S. Diao, Z. Liu, and S. Pan, Reliable memristor based on ultrathin native silicon oxide, *ACS Appl. Mater. Interfaces* 14(18), 21207 (2022)
27. A. N. Mikhaylov, A. I. Belov, D. V. Guseinov, D. S. Korolev, I. N. Antonov, D. V. Efimovykh, S. V. Tikhov, A. P. Kasatkin, O. N. Gorshkov, D. I. Tetelbaum, A. I. Bobrov, N. V. Malekhonova, D. A. Pavlov, E. G. Gryaznov, and A. P. Yatmanov, Bipolar resistive switching and charge transport in silicon oxide memristor, *Mater. Sci. Eng. B* 194, 48 (2015)
28. Q. Gao, A. Huang, Q. Hu, X. Zhang, Y. Chi, R. Li, Y. Ji, X. Chen, R. Zhao, M. Wang, H. Shi, M. Wang, Y. Cui, Z. Xiao, and P. K. Chu, Stability and repeatability of a Karst-like hierarchical porous silicon oxide-based memristor, *ACS Appl. Mater. Interfaces* 11(24), 21734 (2019)
29. S. Kim, H. Kim, S. Hwang, M. H. Kim, Y. F. Chang, and B. G. Park, Analog synaptic behavior of a silicon nitride memristor, *ACS Appl. Mater. Interfaces* 9(46), 40420 (2017)
30. S. Kim, S. Jung, M. H. Kim, Y. C. Chen, Y. F. Chang, K. C. Ryoo, S. Cho, J. H. Lee, and B. G. Park, Scaling effect on silicon nitride memristor with highly doped Si substrate, *Small* 14(19), 1704062 (2018)
31. D. Kim, S. Kim, and S. Kim, Logic-in-memory application of CMOS compatible silicon nitride memristor, *Chaos Solitons Fractals* 153, 111540 (2021)
32. A. A. Gismatulin, V. A. Gritsenko, T. J. Yen, and A. Chin, Charge transport mechanism in SiN_x-based memristor, *Appl. Phys. Lett.* 115(25), 253502 (2019)
33. A. A. Gismatulin, O. M. Orlov, V. A. Gritsenko, V. N. Kruchinin, D. S. Mizginov, and G. Y. Krasnikov, Charge transport mechanism in the metal–nitride–oxide–silicon forming-free memristor structure, *Appl. Phys. Lett.* 116(20), 203502 (2020)
34. R. Schmitt, M. Kubicek, E. Sediva, M. Trassin, M. C. Weber, A. Rossi, H. Hutter, J. Kreisel, M. Fiebig, and J. L. M. Rupp, Accelerated ionic motion in amorphous memristor oxides for nonvolatile memories and neuromorphic computing, *Adv. Funct. Mater.* 29(5), 1804782 (2019)
35. Q. Lu, Y. Chen, H. Bluhm, and B. Yildiz, Electronic structure evolution of $SrCoO_x$ during electrochemically driven phase transition probed by in situ X-ray spectroscopy, *J. Phys. Chem. C* 120(42), 24148 (2016)
36. H. Nili, T. Ahmed, S. Walia, R. Ramanathan, A. E. Kandjani, S. Rubanov, J. Kim, O. Kavehei, V. Bansal, M. Bhaskaran, and S. Sriram, Microstructure and dynamics of vacancy-induced nanofilamentary switching network in donor doped $SrTiO_{3-x}$ memristors, *Nanotechnology* 27(50), 505210 (2016)
37. V. Mikheev, A. Chouprik, Y. Lebedinskii, S. Zarubin, A. M. Markeev, A. V. Zenkevich, and D. Negrov, Memristor with a ferroelectric HfO_2 layer: In which case it is a ferroelectric tunnel junction, *Nanotechnology* 31(21), 215205 (2020)
38. G. U. Siddiqui, M. M. Rehman, and K. H. Choi, Enhanced resistive switching in all-printed, hybrid and flexible memory device based on perovskite $ZnSnO_3$ via PVOH polymer, *Polymer (Guildf.)* 100, 102 (2016)
39. T. Ahmed, S. Walia, E. L. H. Mayes, R. Ramanathan,

P. Guagliardo, V. Bansal, M. Bhaskaran, J. J. Yang, and S. Sriram, Inducing tunable switching behavior in a single memristor, *Appl. Mater. Today* 11, 280 (2018)
40. S. Marinkovic, A. Fernandez-Rodriguez, S. Collienne, S. B. Alvarez, S. Melinte, B. Maiorov, G. Rius, X. Granados, N. Mestres, A. Palau, and A. V. Silhanek, Direct visualization of current-stimulated oxygen migration in $YBa_2Cu_3O_{7-\delta}$ thin films, *ACS Nano* 14(9), 11765 (2020)
41. Z. Shen, C. Zhao, Y. Qi, I. Z. Mitrovic, L. Yang, J. Wen, Y. Huang, P. Li, and C. Zhao, Memristive nonvolatile memory based on graphene materials, *Micromachines (Basel)* 11(4), 341 (2020)
42. H. T. Zhang, T. J. Park, A. N. M. N. Islam, D. S. J. Tran, S. Manna, Q. Wang, S. Mondal, H. Yu, S. Banik, S. Cheng, H. Zhou, S. Gamage, S. Mahapatra, Y. Zhu, Y. Abate, N. Jiang, S. K. R. S. Sankaranarayanan, A. Sengupta, C. Teuscher, and S. Ramanathan, Reconfigurable perovskite nickelate electronics for artificial intelligence, *Science* 375(6580), 533 (2022)
43. B. J. Choi, A. C. Torrezan, J. P. Strachan, P. G. Kotula, A. J. Lohn, M. J. Marinella, Z. Li, R. S. Williams, and J. J. Yang, High-speed and low-energy nitride memristors, *Adv. Funct. Mater.* 26(29), 5290 (2016)
44. B. J. Choi, J. J. Yang, M. X. Zhang, K. J. Norris, D. A. Ohlberg, N. P. Kobayashi, G. Medeiros-Ribeiro, and R. S. Williams, Nitride memristors, *Appl. Phys A* 109(1), 1 (2012)
45. V. K. Perla, S. K. Ghosh, and K. Mallick, Transport mechanism of copper sulfide embedded carbon nitride thin films: A formation free memristor, *Mater. Adv.* 1(2), 228 (2020)
46. W. Zhang, H. Gao, C. Deng, T. Lv, S. Hu, H. Wu, S. Xue, Y. Tao, L. Deng, and W. Xiong, An ultrathin memristor based on a two-dimensional WS_2/MoS_2 heterojunction, *Nanoscale* 13(26), 11497 (2021)
47. A. N. Belov, A. A. Golishnikov, A. M. Mastinin, A. A. Perevalov, and V. I. Shevyakov, Study of the formation process of memristor structures based on copper sulfide, *Semiconductors* 53(15), 2024 (2019)
48. M. Patel, N. R. Hemanth, J. Gosai, R. Mohili, A. Solanki, M. Roy, B. Fang, and N. K. Chaudhari, Mxenes: Promising 2D memristor materials for neuromorphic computing components, *Trends Chem.* 4(9), 835 (2022)
49. N. He, X. Liu, F. Gao, Q. Zhang, M. Zhang, Y. Wang, X. Shen, X. Wan, X. Lian, E. Hu, L. He, J. Xu, and Y. Tong, Demonstration of 2D mxene memristor: Stability, conduction mechanism, and synaptic plasticity, *Mater. Lett.* 266, 127413 (2020)
50. K. Wang, Y. Jia, and X. Yan, A biomimetic afferent nervous system based on the flexible artificial synapse, *Nano Energy* 100, 107486 (2022)
51. Y. Qi, B. Sun, G. Fu, T. Li, S. Zhu, L. Zheng, S. Mao, X. Kan, M. Lei, and Y. Chen, A nonvolatile organic resistive switching memory based on lotus leaves, *Chem. Phys.* 516, 168 (2019)
52. T. Berzina, A. Smerieri, M. Bernabò, A. Pucci, G. Ruggeri, V. Erokhin, and M. P. Fontana, Optimization of an organic memristor as an adaptive memory element, *J. Appl. Phys.* 105(12), 124515 (2009)
53. K. Sun, J. Chen, and X. Yan, The future of memristors: Materials engineering and neural networks, *Adv. Funct. Mater.* 31(8), 2006773 (2021)
54. K. Nasrin, V. Sudharshan, K. Subramani, and M. Sathish, Insights into 2D/2D MXene heterostructures for improved synergy in structure toward next-generation supercapacitors: A review, *Adv. Funct. Mater.* 32(18), 2110267 (2022)
55. X. Feng, Z. Yu, Y. Sun, M. Shan, R. Long, and X. Li, 3D MXene/Ag_2S material as schottky junction catalyst with stable and enhanced photocatalytic activity and photocorrosion resistance, *Separ. Purif. Tech.* 266, 118606 (2021)
56. L. Zhang, K. Khan, J. Zou, H. Zhang, and Y. Li, Recent advances in emerging 2D material-based gas sensors: Potential in disease diagnosis, *Adv. Mater. Interfaces* 6(22), 1901329 (2019)
57. G. Jonker and J. Van Santen, Ferromagnetic compounds of manganese with perovskite structure, *Physica* 16(3), 337 (1950)
58. D. N. Jeong, J. M. Yang, and N. G. Park, Roadmap on halide perovskite and related devices, *Nanotechnology* 31(15), 152001 (2020)
59. Y. Fang, S. Zhai, L. Chu, and J. Zhong, Advances in halide perovskite memristor from lead-based to lead-free materials, *ACS Appl. Mater. Interfaces* 13(15), 17141 (2021)
60. K. Yan, B. Dong, X. Xiao, S. Chen, B. Chen, X. Gao, H. Hu, W. Wen, J. Zhou, and D. Zou, Memristive property's effects on the *I–V* characteristics of perovskite solar cells, *Sci. Rep.* 7(1), 6025 (2017)
61. H. J. Gogoi and A. T. Mallajosyula, Enhancing the switching performance of $CH_3NH_3PbI_3$ memristors by the control of size and characterization parameters, *Adv. Electron. Mater.* 7(11), 2100472 (2021)
62. K. J. Kwak, J. H. Baek, D. E. Lee, I. H. Im, J. Kim, S. J. Kim, Y. J. Lee, J. Y. Kim, and H. W. Jang, Ambient stable all inorganic $CsCu_2I_3$ artificial synapses for neurocomputing, *Nano Lett.* 22(14), 6010 (2022)
63. Y. Feng, X. Gao, Y. N. Zhong, J. L. Wu, J. L. Xu, and S. D. Wang, Solution-processed polymer thin-film memristors with an electrochromic feature and frequency-dependent synaptic plasticity, *Adv. Intell. Syst.* 1(3), 1900022 (2019)
64. R. A. John, N. Yantara, Y. F. Ng, G. Narasimman, E. Mosconi, D. Meggiolaro, M. R. Kulkarni, P. K. Gopalakrishnan, C. A. Nguyen, F. De Angelis, S. G. Mhaisalkar, A. Basu, and N. Mathews, Ionotronic halide perovskite drift-diffusive synapses for low-power neuromorphic computation, *Adv. Mater.* 30(51), 1805454 (2018)
65. D. Li, H. Wu, H. C. Cheng, G. Wang, Y. Huang, and X. Duan, Electronic and ionic transport dynamics in organolead halide perovskites, *ACS Nano* 10(7), 6933 (2016)
66. P. Ramasamy, D. H. Lim, B. Kim, S. H. Lee, M. S. Lee, and J. S. Lee, All-inorganic cesium lead halide perovskite nanocrystals for photodetector applications, *Chem. Commun. (Camb.)* 52(10), 2067 (2016)
67. X. Hu, X. Zhang, L. Liang, J. Bao, S. Li, W. Yang,

and Y. Xie, High-performance flexible broadband photodetector based on organolead halide perovskite, *Adv. Funct. Mater.* 24(46), 7373 (2014)
68. E. Joseph, S. P. Madhusudanan, K. Mohanta, M. Karthega, and S. K. Batabyal, Multiple negative differential resistance in perovskite ($CH_3NH_3PbI_3$) decorated electrospun TiO_2 nanofibers, *Appl. Phys A* 126(9), 707 (2020)
69. D. Hao, J. Zhang, S. Dai, J. Zhang, and J. Huang, Perovskite/organic semiconductor-based photonic synaptic transistor for artificial visual system, *ACS Appl. Mater. Interfaces* 12(35), 39487 (2020)
70. P. Wang, X. Bai, C. Sun, X. Zhang, T. Zhang, and Y. Zhang, Multicolor fluorescent light-emitting diodes based on cesium lead halide perovskite quantum dots, *Appl. Phys. Lett.* 109(6), 063106 (2016)
71. Y. Sun, L. Qian, D. Xie, Y. Lin, M. Sun, W. Li, L. Ding, T. Ren, and T. Palacios, Photoelectric synaptic plasticity realized by 2D perovskite, *Adv. Funct. Mater.* 29(28), 1902538 (2019)
72. Y. Sun, et al., Research progress of solution processed all-inorganic perovskite solar cell, *Acta Phys. Sin.* 68(15), 158806 (2019)
73. Q. You, F. Huang, F. Fang, J. Zhu, Y. Zheng, S. Fang, B. Zhou, H. Li, C. Han, and Y. Shi, Controllable volatile-to-nonvolatile memristive switching in single-crystal lead-free double perovskite with ultralow switching electric field, *Sci. China Mater.* 66(1), 241 (2023)
74. L. Protesescu, S. Yakunin, M. I. Bodnarchuk, F. Krieg, R. Caputo, C. H. Hendon, R. X. Yang, A. Walsh, and M. V. Kovalenko, Nanocrystals of cesium lead halide perovskites ($CsPbX_3$, X = Cl, Br, and I): Novel optoelectronic materials showing bright emission with wide color gamut, *Nano Lett.* 15(6), 3692 (2015)
75. B. D. Folie, J. A. Tan, J. Huang, P. C. Sercel, M. Delor, M. Lai, J. L. Lyons, N. Bernstein, A. L. Efros, P. Yang, and N. S. Ginsberg, Effect of anisotropic confinement on electronic structure and dynamics of band edge excitons in inorganic perovskite nanowires, *J. Phys. Chem. A* 124(9), 1867 (2020)
76. P. Li, Y. Chen, T. Yang, Z. Wang, H. Lin, Y. Xu, L. Li, H. Mu, B. N. Shivananju, Y. Zhang, Q. Zhang, A. Pan, S. Li, D. Tang, B. Jia, H. Zhang, and Q. Bao, Two-dimensional $CH_3NH_3PbI_3$ perovskite nanosheets for ultrafast pulsed fiber lasers, *ACS Appl. Mater. Interfaces* 9(14), 12759 (2017)
77. X. Liu, Y. Wang, T. Wu, X. He, X. Meng, J. Barbaud, H. Chen, H. Segawa, X. Yang, and L. Han, Efficient and stable tin perovskite solar cells enabled by amorphous-polycrystalline structure, *Nat. Commun.* 11(1), 2678 (2020)
78. M. M. Lee, J. Teuscher, T. Miyasaka, T. N. Murakami, and H. J. Snaith, Efficient hybrid solar cells based on meso-superstructured organometal halide perovskites, *Science* 338(6107), 643 (2012)
79. H. S. Kim, C. R. Lee, J. H. Im, K. B. Lee, T. Moehl, A. Marchioro, S. J. Moon, R. Humphry-Baker, J. H. Yum, J. E. Moser, M. Grätzel, and N. G. Park, Lead iodide perovskite sensitized all-solid-state submicron thin film mesoscopic solar cell with efficiency exceeding 9%, *Sci. Rep.* 2(1), 591 (2012)
80. A. Kojima, K. Teshima, Y. Shirai, and T. Miyasaka, Organometal halide perovskites as visible-light sensitizers for photovoltaic cells, *J. Am. Chem. Soc.* 131(17), 6050 (2009)
81. NREL, Best Research-Cell Efficiency Chart, URL: www.nrel.gov/pv/cell-efficiency.html
82. L. C. Schmidt, A. Pertegás, S. González-Carrero, O. Malinkiewicz, S. Agouram, G. Minguez Espallargas, H. J. Bolink, R. E. Galian, and J. Pérez-Prieto, Nontemplate synthesis of $CH_3NH_3PbBr_3$ perovskite nanoparticles, *J. Am. Chem. Soc.* 136(3), 850 (2014)
83. Y. H. Kim, J. S. Kim, and T. W. Lee, Strategies to improve luminescence efficiency of metal-halide perovskites and light-emitting diodes, *Adv. Mater.* 31(47), 1804595 (2019)
84. H. C. Wang, W. Wang, A. C. Tang, H. Y. Tsai, Z. Bao, T. Ihara, N. Yarita, H. Tahara, Y. Kanemitsu, S. Chen, and R. S. Liu, High-performance $CsPb_{1-x}Sn_xBr_3$ perovskite quantum dots for light-emitting diodes, *Angew. Chem.* 129(44), 13838 (2017)
85. L. Basiricò, A. Ciavatti, and B. Fraboni, Solution-grown organic and perovskite X-ray detectors: A new paradigm for the direct detection of ionizing radiation, *Adv. Mater. Technol.* 6(1), 2000475 (2021)
86. M. Ahmadi, T. Wu, and B. Hu, A review on organic–inorganic halide perovskite photodetectors: Device engineering and fundamental physics, *Adv. Mater.* 29(41), 1605242 (2017)
87. S. F. Leung, K. T. Ho, P. K. Kung, V. K. S. Hsiao, H. N. Alshareef, Z. L. Wang, and J. H. He, A self-powered and flexible organometallic halide perovskite photodetector with very high detectivity, *Adv. Mater.* 30(8), 1704611 (2018)
88. Y. H. Kim, S. Kim, A. Kakekhani, J. Park, J. Park, Y. H. Lee, H. Xu, S. Nagane, R. B. Wexler, D. H. Kim, S. H. Jo, L. Martínez-Sarti, P. Tan, A. Sadhanala, G. S. Park, Y. W. Kim, B. Hu, H. J. Bolink, S. Yoo, R. H. Friend, A. M. Rappe, and T. W. Lee, Comprehensive defect suppression in perovskite nanocrystals for high-efficiency light-emitting diodes, *Nat. Photonics* 15(2), 148 (2021)
89. M. Hu, S. Jia, Y. Liu, J. Cui, Y. Zhang, H. Su, S. Cao, L. Mo, D. Chu, G. Zhao, K. Zhao, Z. Yang, and S. F. Liu, Large and dense organic–inorganic hybrid perovskite $CH_3NH_3PbI_3$ wafer fabricated by one-step reactive direct wafer production with high X-ray sensitivity, *ACS Appl. Mater. Interfaces* 12(14), 16592 (2020)
90. W. Tress, N. Marinova, T. Moehl, S. M. Zakeeruddin, M. K. Nazeeruddin, and M. Grätzel, Understanding the rate-dependent *J–V* hysteresis, slow time component, and aging in $CH_3NH_3PbI_3$ perovskite solar cells: The role of a compensated electric field, *Energy Environ. Sci.* 8(3), 995 (2015)
91. Y. Shao, Z. Xiao, C. Bi, Y. Yuan, and J. Huang, Origin and elimination of photocurrent hysteresis by fullerene passivation in $CH_3NH_3PbI_3$ planar heterojunction solar cells, *Nat. Commun.* 5(1), 5784 (2014)
92. E. L. Unger, E. T. Hoke, C. D. Bailie, W. H. Nguyen, A. R. Bowring, T. Heumüller, M. G. Christoforo, and

M. D. Mcgehee, Hysteresis and transient behavior in current–voltage measurements of hybrid-perovskite absorber solar cells, *Energy Environ. Sci.* 7(11), 3690 (2014)
93. W. S. Yang, B. W. Park, E. H. Jung, N. J. Jeon, Y. C. Kim, D. U. Lee, S. S. Shin, J. Seo, E. K. Kim, J. H. Noh, and S. I. Seok, Iodide management in formamidinium-lead-halide-based perovskite layers for efficient solar cells, *Science* 356(6345), 1376 (2017)
94. Y. Yu, J. Li, D. Geng, J. Wang, L. Zhang, T. L. Andrew, M. S. Arnold, and X. Wang, Development of lead iodide perovskite solar cells using three-dimensional titanium dioxide nanowire architectures, *ACS Nano* 9(1), 564 (2015)
95. R. S. Sanchez, V. Gonzalez-Pedro, J. W. Lee, N. G. Park, Y. S. Kang, I. Mora-Sero, and J. Bisquert, Slow dynamic processes in lead halide perovskite solar cells: Characteristic times and hysteresis, *J. Phys. Chem. Lett.* 5(13), 2357 (2014)
96. J. H. Heo, D. H. Song, H. J. Han, S. Y. Kim, J. H. Kim, D. Kim, H. W. Shin, T. K. Ahn, C. Wolf, T. W. Lee, and S. H. Im, Planar $CH_3NH_3PbI_3$ perovskite solar cells with constant 17.2% average power conversion efficiency irrespective of the scan rate, *Adv. Mater.* 27(22), 3424 (2015)
97. P. Zawal, T. Mazur, M. Lis, A. Chiolerio, and K. Szacilowski, Light-induced synaptic effects controlled by incorporation of charge-trapping layer into hybrid perovskite memristor, *Adv. Electron. Mater.* 8(4), 2100838 (2022)
98. C. Eames, J. M. Frost, P. R. F. Barnes, B. C. O'regan, A. Walsh, and M. S. Islam, Ionic transport in hybrid lead iodide perovskite solar cells, *Nat. Commun.* 6(1), 7497 (2015)
99. J. M. Azpiroz, E. Mosconi, J. Bisquert, and F. De Angelis, Defect migration in methylammonium lead iodide and its role in perovskite solar cell operation, *Energy Environ. Sci.* 8(7), 2118 (2015)
100. P. Liu, W. Wang, S. Liu, H. Yang, and Z. Shao, Fundamental understanding of photocurrent hysteresis in perovskite solar cells, *Adv. Energy Mater.* 9(13), 1803017 (2019)
101. H. Kim, J. S. Han, J. Choi, S. Y. Kim, and H. W. Jang, Halide perovskites for applications beyond photovoltaics, *Small Methods* 2(3), 1700310 (2018)
102. T. Li, H. Yu, S. H. Y. Chen, Y. Zhou, and S. T. Han, The strategies of filament control for improving the resistive switching performance, *J. Mater. Chem. C* 8(46), 16295 (2020)
103. T. Li, H. Yu, Z. Xiong, Z. Gao, Y. Zhou, and S. T. Han, 2D oriented covalent organic frameworks for alcohol-sensory synapses, *Mater. Horiz.* 8(7), 2041 (2021)
104. Y. Yang, W. Gao, Z. Xie, Y. Wang, G. Yuan, and J. M. Liu, An all-inorganic, transparent, flexible, and nonvolatile resistive memory, *Adv. Electron. Mater.* 4(12), 1800412 (2018)
105. X. Tian, L. Wang, J. Wei, S. Yang, W. Wang, Z. Xu, and X. Bai, Filament growth dynamics in solid electrolyte-based resistive memories revealed by *in situ* tem, *Nano Res.* 7(7), 1065 (2014)
106. J. Chen, Z. Feng, M. Luo, J. Wang, Z. Wang, Y. Gong, S. Huang, F. Qian, Y. Zhou, and S. T. Han, High-performance perovskite memristor by integrating a tip-shape contact, *J. Mater. Chem. C* 9(43), 15435 (2021)
107. H. L. Park, M. H. Kim, and S. H. Lee, Introduction of interfacial load polymeric layer to organic flexible memristor for regulating conductive filament growth, *Adv. Electron. Mater.* 6(10), 2000582 (2020)
108. Q. Chen, M. Lin, Z. Wang, X. Zhao, Y. Cai, Q. Liu, Y. Fang, Y. Yang, M. He, and R. Huang, Low power parylene-based memristors with a graphene barrier layer for flexible electronics applications, *Adv. Electron. Mater.* 5(9), 1800852 (2019)
109. E. Yoo, M. Lyu, J. H. Yun, C. Kang, Y. Choi, and L. Wang, Bifunctional resistive switching behavior in an organolead halide perovskite based Ag/$CH_3NH_3PbI_{3-x}Cl_x$/FTO structure, *J. Mater. Chem. C* 4(33), 7824 (2016)
110. J. Choi, Q. V. Le, K. Hong, C. W. Moon, J. S. Han, K. C. Kwon, P. R. Cha, Y. Kwon, S. Y. Kim, and H. W. Jang, Enhanced endurance organolead halide perovskite resistive switching memories operable under an extremely low bending radius, *ACS Appl. Mater. Interfaces* 9(36), 30764 (2017)
111. S. Lee, S. Wolfe, J. Torres, M. Yun, and J. K. Lee, Asymmetric bipolar resistive switching of halide perovskite film in contact with TiO_2 layer, *ACS Appl. Mater. Interfaces* 13(23), 27209 (2021)
112. B. Ku, B. Koo, A. S. Sokolov, M. J. Ko, and C. Choi, Two-terminal artificial synapse with hybrid organic-inorganic perovskite $(CH_3NH_3)PbI_3$ and low operating power energy (similar to 47 fJ/μm^2), *J. Alloys Compd.* 833, 155064 (2020)
113. C. Gonzales and A. Guerrero, Mechanistic and kinetic analysis of perovskite memristors with buffer layers: The case of a two-step set process, *J. Phys. Chem. Lett.* 14(6), 1395 (2023)
114. H. Tan, G. Liu, X. Zhu, H. Yang, B. Chen, X. Chen, J. Shang, W. D. Lu, Y. Wu, and R. W. Li, An optoelectronic resistive switching memory with integrated demodulating and arithmetic functions, *Adv. Mater.* 27(17), 2797 (2015)
115. W. Ruan, Y. Hu, T. Qiu, F. Bai, S. Zhang, and F. Xu, Morphological regulation of all-inorganic perovskites for multilevel resistive switching, *J. Phys. Chem. Solids* 127, 258 (2019)
116. S. Ge, X. Guan, Y. Wang, C. H. Lin, Y. Cui, Y. Huang, X. Zhang, R. Zhang, X. Yang, and T. Wu, Low-dimensional lead-free inorganic perovskites for resistive switching with ultralow bias, *Adv. Funct. Mater.* 30(25), 2002110 (2020)
117. S. Paramanik, A. Maiti, S. Chatterjee, and A. J. Pal, Large resistive switching and artificial synaptic behaviors in layered $Cs_3Sb_2I_9$ lead-free perovskite memory devices, *Adv. Electron. Mater.* 8(1), 2100237 (2022)
118. Z. Liu, P. Cheng, Y. Li, R. Kang, J. Zhou, J. Zhao, and Z. Zuo, Multilevel halide perovskite memristors based on optical & electrical resistive switching effects, *Mater. Chem. Phys.* 288, 126393 (2022)
119. S. Wu, L. Ren, J. Qing, F. Yu, K. Yang, M. Yang, Y. Wang, M. Meng, W. Zhou, X. Zhou, and S. Li, Bipolar resistance switching in transparent ITO/$LaAlO_3$/

$SrTiO_3$ memristors, *ACS Appl. Mater. Interfaces* 6(11), 8575 (2014)
120. H. Nili, S. Walia, S. Balendhran, D. B. Strukov, M. Bhaskaran, and S. Sriram, Nanoscale resistive switching in amorphous perovskite oxide (a-$SrTiO_3$) memristors, *Adv. Funct. Mater.* 24(43), 6741 (2014)
121. J. S. Han, Q. V. Le, J. Choi, H. Kim, S. G. Kim, K. Hong, C. W. Moon, T. L. Kim, S. Y. Kim, and H. W. Jang, Lead-free all-inorganic cesium tin iodide perovskite for filamentary and interface-type resistive switching toward environment-friendly and temperature-tolerant nonvolatile memories, *ACS Appl. Mater. Interfaces* 11(8), 8155 (2019)
122. J. Xu, Y. Wu, Z. Li, X. Liu, G. Cao, and J. Yao, Resistive switching in nonperovskite-phase $CsPbI_3$ film-based memory devices, *ACS Appl. Mater. Interfaces* 12(8), 9409 (2020)
123. X. Zhang, H. Yang, Z. Jiang, Y. Zhang, S. Wu, H. Pan, N. Khisro, and X. Chen, Photoresponse of nonvolatile resistive memory device based on all-inorganic perovskite $CsPbBr_3$ nanocrystals, *J. Phys. D* 52(12), 125103 (2019)
124. B. Cho, S. Song, Y. Ji, T. W. Kim, and T. Lee, Organic resistive memory devices: Performance enhancement, integration, and advanced architectures, *Adv. Funct. Mater.* 21(15), 2806 (2011)
125. P. N. Murgatroyd, Theory of space-charge-limited current enhanced by Frenkel effect, *J. Phys. D* 3(2), 151 (1970)
126. Q. Luo, X. Zhang, Y. Hu, T. Gong, X. Xu, P. Yuan, H. Ma, D. Dong, H. Lv, S. Long, Q. Liu, and M. Liu, Self-rectifying and forming-free resistive-switching device for embedded memory application, *IEEE Electron Device Lett.* 39(5), 664 (2018)
127. B. S. Anjali, B. S. Patial, and N. Thakur, High field conduction in Pb doped amorphous Se–Te system, *AIP Conf. Proc.* 1953(1), 090032 (2018)
128. Z. H. Liu, G. I. Ng, S. Arulkumaran, Y. K. T. Maung, and H. Zhou, Temperature-dependent forward gate current transport in atomic-layer-deposited Al_2O_3/AlGaN/GaN metal–insulator–semiconductor high electron mobility transistor, *Appl. Phys. Lett.* 98(16), 163501 (2011)
129. C. Xu, B. Zhang, A. C. Wang, W. Cai, Y. Zi, P. Feng, and Z. L. Wang, Effects of metal work function and contact potential difference on electron thermionic emission in contact electrification, *Adv. Funct. Mater.* 29(29), 1903142 (2019)
130. W. Li, D. Jena, and H. G. Xing, A unified thermionic and thermionic-field emission (TE–TFE) model for ideal Schottky reverse-bias leakage current, *J. Appl. Phys.* 131(1), 015702 (2022)
131. S. Kunwar, C. B. Somodi, R. A. Lalk, B. X. Rutherford, Z. Corey, P. Roy, D. Zhang, M. Hellenbrand, M. Xiao, J. L. Macmanus-Driscoll, Q. Jia, H. Wang, J. Joshua Yang, W. Nie, and A. Chen, Protons: Critical species for resistive switching in interface-type memristors *Adv. Electron. Mater.* 9(1), 2200816 (2023)
132. S. Bagdzevicius, K. Maas, M. Boudard, and M. Burriel, Interface-type resistive switching in perovskite materials, *J. Electroceram.* 39(1–4), 157 (2017)
133. D. Drozdowski, A. Gągor, D. Stefańska, J. K. Zaręba, K. Fedoruk, M. Mączka, and A. Sieradzki, Three-dimensional methylhydrazinium lead halide perovskites: Structural changes and effects on dielectric, linear, and nonlinear optical properties entailed by the halide tuning, *J. Phys. Chem. C* 126(3), 1600 (2022)
134. G. Tang, Z. Xiao, and J. Hong, Designing two-dimensional properties in three-dimensional halide perovskites via orbital engineering, *J. Phys. Chem. Lett.* 10(21), 6688 (2019)
135. B. Saparov and D. B. Mitzi, Organic–inorganic perovskites: Structural versatility for functional materials design, *Chem. Rev.* 116(7), 4558 (2016)
136. S. Tao, I. Schmidt, G. Brocks, J. Jiang, I. Tranca, K. Meerholz, and S. Olthof, Absolute energy level positions in tin- and lead-based halide perovskites, *Nat. Commun.* 10(1), 2560 (2019)
137. R. L. Z. Hoye, J. Hidalgo, R. A. Jagt, J. P. Correa-Baena, T. Fix, and J. L. Macmanus-Driscoll, The role of dimensionality on the optoelectronic properties of oxide and halide perovskites, and their halide derivatives, *Adv. Energy Mater.* 12(4), 2100499 (2022)
138. Y. Deng, E. Peng, Y. Shao, Z. Xiao, Q. Dong, and J. Huang, Scalable fabrication of efficient organolead trihalide perovskite solar cells with doctor-bladed active layers, *Energy Environ. Sci.* 8(5), 1544 (2015)
139. Z. Xiao, C. Bi, Y. Shao, Q. Dong, Q. Wang, Y. Yuan, C. Wang, Y. Gao, and J. Huang, Efficient, high yield perovskite photovoltaic devices grown by interdiffusion of solution-processed precursor stacking layers, *Energy Environ. Sci.* 7(8), 2619 (2014)
140. A. Miyata, A. Mitioglu, P. Plochocka, O. Portugall, J. T. W. Wang, S. D. Stranks, H. J. Snaith, and R. J. Nicholas, Direct measurement of the exciton binding energy and effective masses for charge carriers in organic–inorganic tri-halide perovskites, *Nat. Phys.* 11(7), 582 (2015)
141. C. C. Stoumpos and M. G. Kanatzidis, Halide perovskites: Poor man's high-performance semiconductors, *Adv. Mater.* 28(28), 5778 (2016)
142. X. Zhao, H. Xu, Z. Wang, Y. Lin, and Y. Liu, Memristors with organic-inorganic halide perovskites, *InfoMat* 1(2), 183 (2019)
143. Y. Liu, L. A. Renna, H. B. Thompson, Z. A. Page, T. Emrick, M. D. Barnes, M. Bag, D. Venkataraman, and T. P. Russell, Role of ionic functional groups on ion transport at perovskite interfaces, *Adv. Energy Mater.* 7(21), 1701235 (2017)
144. V. Gupta, G. Lucarelli, S. Castro-Hermosa, T. Brown, and M. Ottavi, Investigation of hysteresis in hole transport layer free metal halide perovskites cells under dark conditions, *Nanotechnology* 31(44), 445201 (2020)
145. F. Haque, and M. Mativenga, Halide perovskite memtransistor enabled by ion migration, *Jpn. J. Appl. Phys.* 59(8), 081002 (2020)
146. H. Patil, H. Kim, K. D. Kadam, S. Rehman, S. A. Patil, J. Aziz, T. D. Dongale, Z. Ali Sheikh, M. Khalid Rahmani, M. F. Khan, and D. K. Kim, Flexible organic–inorganic halide perovskite-based diffusive memristor for artificial nociceptors, *ACS Appl. Mater.*

Interfaces 15(10), 13238 (2023)
147. J. Q. Yang, R. Wang, Z. P. Wang, Q. Y. Ma, J. Y. Mao, Y. Ren, X. Yang, Y. Zhou, and S. T. Han, Leaky integrate-and-fire neurons based on perovskite memristor for spiking neural networks, *Nano Energy* 74, 104828 (2020)
148. N. M. Samardzic, J. S. Bajic, D. L. Sekulic, and S. Dautovic, Volatile memristor in leaky integrate-and-fire neurons: Circuit simulation and experimental study, *Electronics (Basel)* 11(6), 894 (2022)
149. T. J. Lee, S. K. Kim, and T. Y. Seong, Sputtering-deposited amorphous $SrVO_x$-based memristor for use in neuromorphic computing, *Sci. Rep.* 10(1), 5761 (2020)
150. Y. Gong, X. Xing, Z. Lv, J. Chen, P. Xie, Y. Wang, S. Huang, Y. Zhou, and S. T. Han, Ultrasensitive flexible memory phototransistor with detectivity of 1.8×10^{13} Jones for artificial visual nociceptor, *Adv. Intell. Syst.* 4(8), 2100257 (2022)
151. R. A. John, N. Yantara, S. E. Ng, M. I. B. Patdillah, M. R. Kulkarni, N. F. Jamaludin, J. Basu, S. G. Ankit, S. G. Mhaisalkar, A. Basu, and N. Mathews, Diffusive and drift halide perovskite memristive barristors as nociceptive and synaptic emulators for neuromorphic computing, *Adv. Mater.* 33(15), 2007851 (2021)
152. U. Das, P. Sarkar, B. Paul, and A. Roy, Halide perovskite two-terminal analog memristor capable of photo-activated synaptic weight modulation for neuromorphic computing, *Appl. Phys. Lett.* 118(18), 182103 (2021)
153. S. Wang, Y. Xiong, X. Dong, J. Sha, Y. Wu, W. Li, and Y. Wang, Capacitive coupling behaviors based on triple cation organic–inorganic hybrid perovskite memristor *J. Alloys Compd.* 874, 159884 (2021)
154. G. Zhou, B. Sun, Z. Ren, L. Wang, C. Xu, B. Wu, P. Li, Y. Yao, and S. Duan, Resistive switching behaviors and memory logic functions in single MnO_x nanorod modulated by moisture, *Chem. Commun. (Camb.)* 55(67), 9915 (2019)
155. M. A. Haque, A. Syed, F. H. Akhtar, R. Shevate, S. Singh, K. V. Peinemann, D. Baran, and T. Wu, Giant humidity effect on hybrid halide perovskite microstripes: Reversibility and sensing mechanism *ACS Appl. Mater. Interfaces* 11(33), 29821 (2019)
156. A. M. A. Leguy, Y. Hu, M. Campoy-Quiles, M. I. Alonso, O. J. Weber, P. Azarhoosh, M. Van Schilfgaarde, M. T. Weller, T. Bein, J. Nelson, P. Docampo, and P. R. F. Barnes, Reversible hydration of $CH_3NH_3PbI_3$ in films, single crystals, and solar cells, *Chem. Mater.* 27(9), 3397 (2015)
157. X. Zhang, X. Zhao, X. Shan, Q. Tian, Z. Wang, Y. Lin, H. Xu, and Y. Liu, Humidity effect on resistive switching characteristics of the $CH_3NH_3PbI_3$ memristor, *ACS Appl. Mater. Interfaces* 13(24), 28555 (2021)
158. M. Kulbak, D. Cahen, and G. Hodes, How important is the organic part of lead halide perovskite photovoltaic cells? Efficient $CsPbBr_3$ cells *J. Phys. Chem. Lett.* 6(13), 2452 (2015)
159. Y. Yin, Z. Yao, Y. Xia, and H. Chen, A method to improve the performance of all-inorganic halide perovskite $CsPbBr_3$ memory, *Mater. Res. Express* 9(6), 065007 (2022)
160. Y. Wang, X. Li, J. Song, L. Xiao, H. Zeng, and H. Sun, All-inorganic colloidal perovskite quantum dots: A new class of lasing materials with favorable characteristics, *Adv. Mater.* 27(44), 7101 (2015)
161. S. Liu, J. Guan, L. Yin, L. Zhou, J. Huang, Y. Mu, S. Han, X. Pi, G. Liu, P. Gao, and S. Zhou, Solution-processed synaptic memristors based on halide perovskite nanocrystals, *J. Phys. Chem. Lett.* 13(47), 10994 (2022)
162. C. Cheng, C. Zhu, B. Huang, H. Zhang, H. Zhang, R. Chen, W. Pei, Q. Chen, and H. Chen, Processing halide perovskite materials with semiconductor technology, *Adv. Mater. Technol.* 4(7), 1800729 (2019)
163. Z. Liu, P. Cheng, Y. Li, R. Kang, Z. Zhang, Z. Zuo, and J. Zhao, High temperature $CsPbBr_xI_{3-x}$ memristors based on hybrid electrical and optical resistive switching effects, *ACS Appl. Mater. Interfaces* 13(49), 58885 (2021)
164. S. Zhai, J. Gong, Y. Feng, Z. Que, W. Mao, X. He, Y. Xie, X. A. Li, and L. Chu, Multilevel resistive switching in stable all-inorganic n–i–p double perovskite memristor, *iScience* 26(4), 106461 (2023)
165. P. D. Dissanayake, K. M. Yeom, B. Sarkar, D. S. Alessi, D. Hou, J. Rinklebe, J. H. Noh, and Y. S. Ok, Environmental impact of metal halide perovskite solar cells and potential mitigation strategies: A critical review, *Environ. Res.* 219, 115066 (2023)
166. Y. Zheng, F. Luo, L. Ruan, J. Tong, L. Yan, C. Sun, and X. Zhang, A facile fabrication of lead-free Cs_2NaBiI_6 double perovskite films for memory device application, *J. Alloys Compd.* 909, 164613 (2022)
167. J. Zhang, S. Han, C. Ji, W. Zhang, Y. Wang, K. Tao, Z. Sun, and J. Luo, $[(CH_3)_3NH]_3Bi_2I_9$: A polar lead-free hybrid perovskite-like material as a potential semiconducting absorber, *Chemistry* 23(68), 17304 (2017)
168. Z. Ni, Y. Zhu, S. Ju, Z. Xu, F. Tian, H. Hu, T. Guo, and F. Li, E-synapse based on lead-free organic halide perovskite $(CH_3NH_3)_3Sb_2Cl_9$ for neuromorphic computing, *IEEE Trans. Electron Dev.* 68(9), 4425 (2021)
169. T. Krishnamoorthy, H. Ding, C. Yan, W. L. Leong, T. Baikie, Z. Zhang, M. Sherburne, S. Li, M. Asta, N. Mathews, and S. G. Mhaisalkar, Lead-free germanium iodide perovskite materials for photovoltaic applications, *J. Mater. Chem. A* 3(47), 23829 (2015)
170. H. Shankar, A. Jha, and P. Kar, Water-assisted synthesis of lead-free Cu based fluorescent halide perovskite nanostructures, *Mater. Adv.* 3(1), 658 (2022)
171. J. C. Hebig, I. Kühn, J. Flohre, and T. Kirchartz, Optoelectronic properties of $(CH_3NH_3)_3Sb_2I_9$ thin films for photovoltaic applications, *ACS Energy Lett.* 1(1), 309 (2016)
172. N. K. Noel, S. D. Stranks, A. Abate, C. Wehrenfennig, S. Guarnera, A. A. Haghighirad, A. Sadhanala, G. E. Eperon, S. K. Pathak, M. B. Johnston, A. Petrozza, L. M. Herz, and H. J. Snaith, Lead-free organic–inorganic tin halide perovskites for photovoltaic applications, *Energy Environ. Sci.* 7(9), 3061 (2014)
173. S. Ge, Y. Wang, Z. Xiang, and Y. Cui, Reset voltage-dependent multilevel resistive switching behavior in

$CsPb_{1-x}Bi_xI_3$ perovskite-based memory device, *ACS Appl. Mater. Interfaces* 10(29), 24620 (2018)

174. W. Ruan, Y. Hu, F. Xu, and S. Zhang, Resistive switching behavior of organic-metallic halide perovskites $CH_3NH_3Pb_{1-x}Bi_xBr_3$, *Org. Electron.* 70, 252 (2019)
175. F. Lv, C. Gao, H. A. Zhou, P. Zhang, K. Mi, and X. Liu, Nonvolatile bipolar resistive switching behavior in the perovskite-like $(CH_3NH_3)_2FeCl_4$, *ACS Appl. Mater. Interfaces* 8(29), 18985 (2016)
176. J. M. Yang, E. S. Choi, S. Y. Kim, J. H. Kim, J. H. Park, and N. G. Park, Perovskite-related $(CH_3NH_3)_3Sb_2Br_9$ for forming-free memristor and low-energy-consuming neuromorphic computing, *Nanoscale* 11(13), 6453 (2019)
177. F. Zeng, Y. Guo, W. Hu, Y. Tan, X. Zhang, J. Feng, and X. Tang, Opportunity of the lead-free all-inorganic $Cs_3Cu_2I_5$ perovskite film for memristor and neuromorphic computing applications, *ACS Appl. Mater. Interfaces* 12(20), 23094 (2020)
178. R. Wang, P. Chen, D. Hao, J. Zhang, Q. Shi, D. Liu, L. Li, L. Xiong, J. Zhou, and J. Huang, Artificial synapses based on lead-free perovskite floating-gate organic field-effect transistors for supervised and unsupervised learning, *ACS Appl. Mater. Interfaces* 13(36), 43144 (2021)
179. J. Lao, W. Xu, C. Jiang, N. Zhong, B. Tian, H. Lin, C. Luo, J. Travas-Sejdic, H. Peng, and C. G. Duan, An air-stable artificial synapse based on a lead-free double perovskite $Cs_2AgBiBr_6$ film for neuromorphic computing, *J. Mater. Chem. C* 9(17), 5706 (2021)
180. C. Wu, Q. Zhang, Y. Liu, W. Luo, X. Guo, Z. Huang, H. Ting, W. Sun, X. Zhong, S. Wei, S. Wang, Z. Chen, and L. Xiao, The dawn of lead-free perovskite solar cell: Highly stable double perovskite $Cs_2AgBiBr_6$ film, *Adv. Sci. (Weinh.)* 5(3), 1700759 (2018)
181. X. F. Cheng, W. H. Qian, J. Wang, C. Yu, J. H. He, H. Li, Q. F. Xu, D. Y. Chen, N. J. Li, and J. M. Lu, Environmentally robust memristor enabled by lead-free double perovskite for high-performance information storage, *Small* 15(49), 1905731 (2019)
182. W. Wang and G. Zhou, Moisture influence in emerging neuromorphic device, *Front. Phys.* 18(5), 53601 (2023)
183. Z. Guo, R. Xiong, Y. Zhu, Z. Wang, J. Zhou, Y. Liu, D. Luo, Y. Wang, and H. Wang, High-performance and humidity robust multilevel lead-free all-inorganic $Cs_3Cu_2Br_5$ perovskite-based memristors, *Appl. Phys. Lett.* 122(5), 053502 (2023)
184. W. H. Qian, X. F. Cheng, J. Zhou, J. H. He, H. Li, Q. F. Xu, N. J. Li, D. Y. Chen, Z. G. Yao, and J. M. Lu, Lead-free perovskite $MASnBr_3$-based memristor for quaternary information storage, *InfoMat* 2(4), 743 (2020)
185. Y. Ren, X. Bu, M. Wang, Y. Gong, J. Wang, Y. Yang, G. Li, M. Zhang, Y. Zhou, and S. T. Han, Synaptic plasticity in self-powered artificial striate cortex for binocular orientation selectivity, *Nat. Commun.* 13(1), 5585 (2022)
186. X. Guan, Z. Lei, X. Yu, C. H. Lin, J. K. Huang, C. Y. Huang, L. Hu, F. Li, A. Vinu, J. Yi, and T. Wu, Low-dimensional metal-halide perovskites as high-performance materials for memory applications, *Small* 18(38), 2203311 (2022)
187. U. Das, P. K. Sarkar, D. Das, B. Paul, and A. Roy, Influence of nanoscale charge trapping layer on the memory and synaptic characteristics of a novel rubidium lead chloride quantum dot based memristor, *Adv. Electron. Mater.* 8(5), 2101015 (2022)
188. C. Gonzales, A. Guerrero, and J. Bisquert, Spectral properties of the dynamic state transition in metal halide perovskite-based memristor exhibiting negative capacitance, *Appl. Phys. Lett.* 118(7), 073501 (2021)
189. S. Batool, M. Idrees, S. R. Zhang, S. T. Han, and Y. Zhou, Novel charm of 2D materials engineering in memristor: When electronics encounter layered morphology, *Nanoscale Horiz.* 7(5), 480 (2022)
190. J. Di, Z. Lin, J. Su, J. Wang, J. Zhang, S. Liu, J. Chang, and Y. Hao, Two-dimensional $(C_6H_5C_2H_4NH_3)_2PbI_4$ perovskite single crystal resistive switching memory devices, *IEEE Electron Device Lett.* 42(3), 327 (2021)
191. J. Liu, K. Chen, S. A. Khan, B. Shabbir, Y. Zhang, Q. Khan, and Q. Bao, Synthesis and optical applications of low dimensional metal-halide perovskites, *Nanotechnology* 31(15), 152002 (2020)
192. S. J. Kim, T. H. Lee, J. M. Yang, J. W. Yang, Y. J. Lee, M. J. Choi, S. A. Lee, J. M. Suh, K. J. Kwak, J. H. Baek, I. H. Im, D. E. Lee, J. Y. Kim, J. Kim, J. S. Han, S. Y. Kim, D. Lee, N. G. Park, and H. W. Jang, Vertically aligned two-dimensional halide perovskites for reliably operable artificial synapses, *Mater. Today* 52, 19 (2022)
193. D. Thrithamarassery Gangadharan, and D. Ma, Searching for stability at lower dimensions: Current trends and future prospects of layered perovskite solar cells, *Energy Environ. Sci.* 12(10), 2860 (2019)
194. H. Tian, L. Zhao, X. Wang, Y. W. Yeh, N. Yao, B. P. Rand, and T. L. Ren, Extremely low operating current resistive memory based on exfoliated 2D perovskite single crystals for neuromorphic computing, *ACS Nano* 11(12), 12247 (2017)
195. M. Kumar, M. Patel, D. Y. Park, H. S. Kim, M. S. Jeong, and J. Kim, Switchable two-terminal transparent optoelectronic devices based on 2D perovskite, *Adv. Electron. Mater.* 5(2), 1800662 (2019)
196. J. M. Yang, S. G. Kim, J. Y. Seo, C. Cuhadar, D. Y. Son, D. Lee, and N. G. Park, 1D hexagonal $HC(NH_2)_2PbI_3$ for multilevel resistive switching nonvolatile memory, *Adv. Electron. Mater.* 4(9), 1800190 (2018)
197. S. Poddar, Y. Zhang, L. Gu, D. Zhang, Q. Zhang, S. Yan, M. Kam, S. Zhang, Z. Song, W. Hu, L. Liao, and Z. Fan, Down-scalable and ultra-fast memristors with ultra-high density three-dimensional arrays of perovskite quantum wires, *Nano Lett.* 21(12), 5036 (2021)
198. G. Zhou, D. Kuang, G. Wang, X. He, C. Xu, J. Dong, Z. Dai, G. Xu, D. Lu, P. Guo, B. Sun, and Q. Song, PbI_3-ion abnormal migration in $CH_3NH_3PbI_xCl_{3-x}$ ultralong single nanowire for resistive switching memories, *Mater. Charact.* 199, 112762 (2023)
199. Z. Chen, Y. Yu, L. Jin, Y. Li, Q. Li, T. Li, Y. Zhang, H. Dai, and J. Yao, Artificial synapses with photoelectric

plasticity and memory behaviors based on charge trapping memristive system, *Mater. Des.* 188, 108415 (2020)
200. Y. Gong, Y. Wang, R. Li, J. Q. Yang, Z. Lv, X. Xing, Q. Liao, J. Wang, J. Chen, Y. Zhou, and S. T. Han, Tailoring synaptic plasticity in a perovskite QD-based asymmetric memristor, *J. Mater. Chem. C* 8(9), 2985 (2020)
201. G. V. Nenashev, A. N. Aleshin, I. P. Shcherbakov, and V. N. Petrov, Effect of temperature variations on the behavior of a two-terminal organic–inorganic halide perovskite rewritable memristor for neuromorphic operations, *Solid State Commun.* 348–349, 114768 (2022)
202. T. K. Su, W. K. Cheng, C. Y. Chen, W. C. Wang, Y. T. Chuang, G. H. Tan, H. C. Lin, C. H. Hou, C. M. Liu, Y. C. Chang, J. J. Shyue, K. C. Wu, and H. W. Lin, Room-temperature fabricated multilevel nonvolatile lead-free cesium halide memristors for reconfigurable in-memory computing, *ACS Nano* 16(8), 12979 (2022)
203. R. A. John, Y. Demirag, Y. Shynkarenko, Y. Berezovska, N. Ohannessian, M. Payvand, P. Zeng, M. I. Bodnarchuk, F. Krumeich, G. Kara, I. Shorubalko, M. V. Nair, G. A. Cooke, T. Lippert, G. Indiveri, and M. V. Kovalenko, Reconfigurable halide perovskite nanocrystal memristors for neuromorphic computing, *Nat. Commun.* 13(1), 2074 (2022)
204. Y. Wang, N. Xu, Y. Yuan, W. Zhang, Q. Huang, X. Tang, and F. Qi, Achieving adjustable digital-to-analog conversion in memristors with embedded $Cs_2AgSbBr_6$ nanoparticles, *Nanoscale* 15(16), 7344 (2023)
205. Z. Zhang, D. Yang, H. Li, C. Li, Z. Wang, L. Sun, and H. Yang, 2d materials and van der waals heterojunctions for neuromorphic computing, *Neuromorph. Comput. Eng.* 2(3), 032004 (2022)
206. Z. Zhou, F. Yang, S. Wang, L. Wang, X. Wang, C. Wang, Y. Xie, and Q. Liu, Emerging of two-dimensional materials in novel memristor, *Front. Phys.* 17(2), 23204 (2022)
207. Q. B. Zhu, B. Li, D. D. Yang, C. Liu, S. Feng, M. L. Chen, Y. Sun, Y. N. Tian, X. Su, X. M. Wang, S. Qiu, Q. W. Li, X. M. Li, H. B. Zeng, H. M. Cheng, and D. M. Sun, A flexible ultrasensitive optoelectronic sensor array for neuromorphic vision systems, *Nat. Commun.* 12(1), 1798 (2021)
208. L. Yin, W. Huang, R. Xiao, W. Peng, Y. Zhu, Y. Zhang, X. Pi, and D. Yang, Optically stimulated synaptic devices based on the hybrid structure of silicon nanomembrane and perovskite, *Nano Lett.* 20(5), 3378 (2020)
209. Y. Wu, Y. Wei, Y. Huang, F. Cao, D. Yu, X. Li, and H. Zeng, Capping $CsPbBr_3$ with ZnO to improve performance and stability of perovskite memristors, *Nano Res.* 10(5), 1584 (2017)
210. Y. Wang, Z. Lv, Q. Liao, H. Shan, J. Chen, Y. Zhou, L. Zhou, X. Chen, V. L. Roy, Z. Wang, Z. Xu, Y. J. Zeng, and S. T. Han, Synergies of electrochemical metallization and valance change in all-inorganic perovskite quantum dots for resistive switching, *Adv. Mater.* 30(28), 1800327 (2018)
211. B. Pradhan, S. Das, J. Li, F. Chowdhury, J. Cherusseri, D. Pandey, D. Dev, A. Krishnaprasad, E. Barrios, A. Towers, A. Gesquiere, L. Tetard, T. Roy, and J. Thomas, Ultrasensitive and ultrathin phototransistors and photonic synapses using perovskite quantum dots grown from graphene lattice, *Sci. Adv.* 6(7), eaay5225 (2020)
212. X. Cheng, Y. Han, and B. B. Cui, Fabrication strategies and optoelectronic applications of perovskite heterostructures, *Adv. Opt. Mater.* 10(5), 2102224 (2022)
213. D. Liu, H. Yu, and Y. Chai, Low-power computing with neuromorphic engineering, *Adv. Intell. Syst.* 3(2), 2000150 (2021)
214. S. J. Kim, S. Kim, and H. W. Jang, Competing memristors for brain-inspired computing, *iScience* 24(1), 101889 (2021)
215. X. Zhu and W. D. Lu, Optogenetics-inspired tunable synaptic functions in memristors, *ACS Nano* 12(2), 1242 (2018)
216. X. Zhao, Z. Wang, W. Li, S. Sun, H. Xu, P. Zhou, J. Xu, Y. Lin, and Y. Liu, Photoassisted electroforming method for reliable low-power organic–inorganic perovskite memristors, *Adv. Funct. Mater.* 30(17), 1910151 (2020)
217. G. Lin, Y. Lin, R. Cui, H. Huang, X. Guo, C. Li, J. Dong, X. Guo, and B. Sun, An organic–inorganic hybrid perovskite logic gate for better computing, *J. Mater. Chem. C* 3(41), 10793 (2015)
218. J. Xing, C. Zhao, Y. Zou, W. Kong, Z. Yu, Y. Shan, Q. Dong, D. Zhou, W. Yu, and C. Guo, Modulating the optical and electrical properties of $MAPbBr_3$ single crystals via voltage regulation engineering and application in memristors, *Light Sci. Appl.* 9(1), 111 (2020)
219. S. Ke, L. Jiang, Y. Zhao, Y. Xiao, B. Jiang, G. Cheng, F. Wu, G. Cao, Z. Peng, M. Zhu, and C. Ye, Brain-like synaptic memristor based on lithium-doped silicate for neuromorphic computing, *Front. Phys.* 17(5), 53508 (2022)
220. A. S. Sokolov, H. Abbas, Y. Abbas, and C. Choi, Towards engineering in memristors for emerging memory and neuromorphic computing: A review, *J. Semicond.* 42(1), 013101 (2021)
221. T. J. Huang, Imitating the brain with neurocomputer a new way towards artificial general intelligence, *Inter. J. Autom. Comput.* 14(5), 520 (2017)
222. F. Zahoor, T. Z. Azni Zulkifli, and F. A. Khanday, Resistive random access memory (RRAM): An overview of materials, switching mechanism, performance, multilevel cell (mlc) storage, modeling, and applications, *Nanoscale Res. Lett.* 15(1), 90 (2020)
223. F. Chen, Y. Zhou, Y. Zhu, R. Zhu, P. Guan, J. Fan, L. Zhou, N. Valanoor, F. Von Wegner, E. Saribatir, I. Birznieks, T. Wan, and D. Chu, Recent progress in artificial synaptic devices: Materials, processing and applications, *J. Mater. Chem. C* 9(27), 8372 (2021)
224. K. J. Kwak, J. H. Baek, D. E. Lee, I. H. Im, J. Kim, S. J. Kim, Y. J. Lee, J. Y. Kim, and H. W. Jang, Ambient stable all inorganic $CsCu_2I_3$ artificial synapses for neurocomputing, *Nano Lett.* 22(14), 6010 (2022)
225. X. Zhu, Q. Wang, and W. D. Lu, Memristor networks

for real-time neural activity analysis, *Nat. Commun.* 11(1), 2439 (2020)
226. W. Huang, P. Hang, Y. Wang, K. Wang, S. Han, Z. Chen, W. Peng, Y. Zhu, M. Xu, Y. Zhang, Y. Fang, X. Yu, D. Yang, and X. Pi, Zero-power optoelectronic synaptic devices, *Nano Energy* 73, 104790 (2020)
227. R. A. John, A. Milozzi, S. Tsarev, R. Brönnimann, S. C. Boehme, E. Wu, I. Shorubalko, M. V. Kovalenko, and D. Ielmini, Ionic-electronic halide perovskite memdiodes enabling neuromorphic computing with a second-order complexity, *Sci. Adv.* 8(51), eade0072 (2022)
228. A. A. Bessonov, M. N. Kirikova, D. I. Petukhov, M. Allen, T. Ryhanen, and M. J. Bailey, Layered memristive and memcapacitive switches for printable electronics, *Nat. Mater.* 14(2), 199 (2015)
229. Y. Lee and T. W. Lee, Organic synapses for neuromorphic electronics: From brain-inspired computing to sensorimotor nervetronics, *Acc. Chem. Res.* 52(4), 964 (2019)
230. X. Yan, X. Han, Z. Fang, Z. Zhao, Z. Zhang, J. Sun, Y. Shao, Y. Zhang, L. Wang, S. Sun, Z. Guo, X. Jia, Y. Zhang, Z. Guan, and T. Shi, Reconfigurable memristor based on $SrTiO_3$ thin-film for neuromorphic computing, *Front. Phys.* 18(6), 63301 (2023)
231. Q. Chen, Y. Zhang, S. Liu, T. Han, X. Chen, Y. Xu, Z. Meng, G. Zhang, X. Zheng, J. Zhao, G. Cao, and G. Liu, Switchable perovskite photovoltaic sensors for bioinspired adaptive machine vision, *Adv. Intell. Syst.* 2(9), 2070092 (2020)
232. X. Yang, Z. Xiong, Y. Chen, Y. Ren, L. Zhou, H. Li, Y. Zhou, F. Pan, and S. T. Han, A self-powered artificial retina perception system for image preprocessing based on photovoltaic devices and memristive arrays, *Nano Energy* 78, 105246 (2020)
233. R. A. John, N. Shah, S. K. Vishwanath, S. E. Ng, B. Febriansyah, M. Jagadeeswararao, C. H. Chang, A. Basu, and N. Mathews, Halide perovskite memristors as flexible and reconfigurable physical unclonable functions, *Nat. Commun.* 12(1), 3681 (2021)
234. H. J. Gogoi, K. Bajpai, A. T. Mallajosyula, and A. Solanki, Advances in flexible memristors with hybrid perovskites, *J. Phys. Chem. Lett.* 12(36), 8798 (2021)
235. K. A. Campbell, Self-directed channel memristor for high temperature operation, *Microelectronics* 59, 10 (2017)
236. K. Song, B. Chen, X. Lin, H. Yang, Y. Liu, Y. Liu, H. Li, and Z. Chen, Thermal enhanced resistive switching performance of ⟨100⟩-oriented perovskite $[(TZ\text{-}H)_2(PbBr_4)]_n$ with high working temperature: A triazolium/$(PbBr_4)_n^{2n-}$ interfacial interaction insight, *Adv. Electron. Mater.* 8(11), 2200537 (2022)
237. A. Soosaimanickam, P. J. Rodríguez-Cantó, J. P. Martínez-Pastor, and R. Abargues, Nanostructured, functional, and flexible materials for energy conversion and storage systems, edited by A. Pandikumar and P. Rameshkumar, Elsevier, 2020, pp 157–228
238. J. Sun, F. Li, J. Yuan, and W. Ma, Advances in metal halide perovskite film preparation: The role of anti-solvent treatment, *Small Methods* 5(5), 2100046 (2021)
239. P. Roy, N. Kumar Sinha, S. Tiwari, and A. Khare, A review on perovskite solar cells: Evolution of architecture, fabrication techniques, commercialization issues and status, *Sol. Energy* 198, 665 (2020)
240. L. Gil-Escrig, C. Momblona, M. G. La-Placa, P. P. Boix, M. Sessolo, and H. J. Bolink, Vacuum deposited triple-cation mixed-halide perovskite solar cells, *Adv. Energy Mater.* 8(14), 1703506 (2018)
241. S. Xie, A. Osherov, and V. Bulović, All-vacuum-deposited inorganic cesium lead halide perovskite light-emitting diodes, *APL Mater.* 8(5), 051113 (2020)
242. N. Zhang, W. Sun, S. P. Rodrigues, K. Wang, Z. Gu, S. Wang, W. Cai, S. Xiao, and Q. Song, Highly reproducible organometallic halide perovskite microdevices based on top-down lithography, *Adv. Mater.* 29(15), 1606205 (2017)
243. S. Parveen, L. T. Manamel, A. Mukherjee, S. Sagar, and B. C. Das, Analog memristor of lead-free $Cs_4CuSb_2Cl_{12}$ layered double perovskite nanocrystals as solid-state electronic synapse for neuromorphic computing, *Adv. Mater. Interfaces* 9(30), 2200562 (2022)